

CECOM-TR-88-P035-F

AD-A284 453



COMPREHENSIVE EVALUATION OF TUNABLE VISIBLE LASER SOURCES

Dr. David C. Brown
Mr. William Gehm
Mr. David Benfey

Laser Technology Associates, Inc.
25 Ozalid Road
Johnson City, NY 13790

Final Report

February 17, 1989

NIGHT VISION & ELECTRONIC SENSORS DIRECTORATE
(NVESD)
AMSEL-RD-NV-SE-EOIR
FORT MONMOUTH, NJ 07703-5206

US Army Contract #DAAB07-88-C-P035

Period Covered July 14, 1988 through January 14, 1989

APPROVED FOR PUBLIC RELEASE;
DISTRIBUTION IS UNLIMITED.

DTIC QUALITY INSPECTED 3

24 9 08 0 58
COMMUNICATIONS-ELECTRONICS COMMAND (CECOM)
FORT MONMOUTH, NJ 07703-5206

DTIC
ELECTE
SEP 09 1990
S B D

61 pg



94-29504

NOTICES

Disclaimers

The findings in this report are not to be construed as an official Department of the Army position, unless so designated by other authorized documents.

The citation of trade names and names of manufacturers in this report is not to be construed as official Government endorsement or approval of commercial products or services referenced herein.

DTIC QUALITY INSPECTED 3

REPORT DOCUMENTATION PAGE			Form Approved OMB No. 0704-0188	
<small>Public reporting burden for this collection of information is estimated to average 1 hour per response, including the time for reviewing instructions, searching existing data sources, gathering and maintaining the data needed, and completing and reviewing the collection of information. Send comments regarding this burden estimate or any other aspect of this collection of information, including suggestions for reducing this burden, to Washington Headquarters Services, Directorate for Information Operations and Reports, 1215 Jefferson Davis Highway, Suite 1204, Arlington, VA 22202-4302, and to the Office of Management and Budget, Paperwork Reduction Project (0704-0188), Washington, DC 20503.</small>				
1. AGENCY USE ONLY (Leave blank)		2. REPORT DATE February 1989	3. REPORT TYPE AND DATES COVERED Final Report: 14 Jul 88 to 14 Jan 89	
4. TITLE AND SUBTITLE COMPREHENSIVE EVALUATION OF TUNABLE VISIBLE LASER SOURCES			5. FUNDING NUMBERS C: DAAB07-88-C-P035	
6. AUTHOR(S) David C. Brown, William Gehm, David Benfey				
7. PERFORMING ORGANIZATION NAME(S) AND ADDRESS(ES) Laser Technology Associates, Inc. 25 Ozalid Road Johnson City, NY 13790			8. PERFORMING ORGANIZATION REPORT NUMBER	
9. SPONSORING/MONITORING AGENCY NAME(S) AND ADDRESS(ES) US Army Communications-Electronics Command (CECOM) Night Vision and Electronic Sensors Directorate ATTN: AMSEL-RD-NV-SE-EOIR (C. Pearce) Fort Monmouth, NJ 07703-5206			10. SPONSORING/MONITORING AGENCY REPORT NUMBER CECOM-TR-88-P035-F	
11. SUPPLEMENTARY NOTES SBIR Phase I Report				
12a. DISTRIBUTION/AVAILABILITY STATEMENT Approved for public release; distribution is unlimited.			12b. DISTRIBUTION CODE	
13. ABSTRACT (Maximum 200 words) <p>We have conducted an evaluation of tunable visible laser sources in the spectral region 0.5-0.6 microns. These included doubled Ti:Sapphire, Ti:YALO, organic dye lasers, and optical parametric oscillators. We conclude that the Ti:Sapphire approach is inefficient in this spectral region, while Ti:YALO cannot be properly evaluated at this time due to a paucity of data. An evaluation of the state-of-the-art in optical parametric oscillators shows that this approach offers the best long-term potential for producing an efficient, compact, all solid-state laser in the visible region. In the near-term, however, the further development of organic dye lasers is warranted given that significant improvements in performance can be obtained by the use of optical phase conjugation and design optimization.</p>				
14. SUBJECT TERMS Dye lasers; optical phase conjugation; Ti:Sapphire; tunable lasers; visible lasers			15. NUMBER OF PAGES 61	
			16. PRICE CODE	
17. SECURITY CLASSIFICATION OF REPORT Unclassified	18. SECURITY CLASSIFICATION OF THIS PAGE Unclassified	19. SECURITY CLASSIFICATION OF ABSTRACT Unclassified	20. LIMITATION OF ABSTRACT UL	

Comprehensive Evaluation of Tunable Visible Laser Sources

FINAL REPORT

Laser Technology Associates, Inc.
25 Ozalid Road
Johnson City, New York 13790
February 17, 1989

U.S. Army Contract Number DAAB07-88-C-P035
Department of the Army
Commander, U.S. Army CECOM
ANSEL-PC-C-D-EW
Fort Monmouth, NJ
07703-5000

Period Covered: July 14, 1988 through January 14, 1989

Persons Preparing Report: Dr. David C. Brown
Mr. William Gehm
Mr. David Benfey

Person Submitting Report: Dr. David C. Brown

Accession For	
NTIS GRA&I	<input checked="" type="checkbox"/>
DTIC TAB	<input type="checkbox"/>
Unannounced	<input type="checkbox"/>
Justification	
By	
Distribution/	
Availability Codes	
Dist	Avail and/or Special
A-1	

The views, opinions, and/or findings contained in this report are those of the author(s) and should not be construed as an official Department of the Army position, policy, or decision, unless designated by other documentation.

The contractor, Laser Technology Associates, Inc., hereby certifies that, to the best of its knowledge and belief, the technical data delivered herewith under Contract No. DAAB07-88-C-P035 is complete, accurate, and complies with all requirements of the contract.

3/24/89

Date

David D. [Signature]

Name and Title of Certifying Official

Comprehensive Evaluation of Tunable Visible Laser Sources

Contents

<u>Section</u>	<u>Page</u>
Abstract	1
I. Introduction	2
II. Executive Summary of Phase I	5
III. Systems Evaluation	6
(a) Ti:YALO	6
(b) Ti:Sapphire	6
(c) Optical Parametric Oscillator	17
(d) Tunable Dye Laser	20
IV. Tunable Dye Laser Modeling	29
(a) Second Harmonic Generation	29
(b) Dye Laser Oscillator Modeling	34
(c) Dye Laser Amplifier Modeling	50
V. Conclusions	53
VI. Summary of Recommended Phase II Program	54
VII. Matching New York State SBIR Program	54
VIII. References	55

Comprehensive Evaluation of Tunable Visible Laser Sources

U.S. Army Contract Number DAAB07-88-C-P035

FINAL REPORT

February 17, 1989

Abstract

We have conducted an evaluation of tunable visible laser sources in the spectral region 0.5-0.6 microns. These included doubled Ti:Sapphire, Ti:YALO, organic dye lasers, and optical parametric oscillators. We conclude that the Ti:Sapphire approach is inefficient in this spectral region, while Ti:YALO cannot be properly evaluated at this time due to a paucity of data. An evaluation of the state-of-the-art in optical parametric oscillators shows that this approach offers the best long-term potential for producing an efficient, compact, all solid-state laser in the visible region. In the near-term, however, the further development of organic dye lasers is warranted given that significant improvements in performance can be obtained by the use of optical phase conjugation and design optimization.

Comprehensive Evaluation of Tunable Visible Laser Sources

I. Introduction

This feasibility study was concerned with tunable visible laser sources, and, in particular, tunable lasers operating in the 0.5-0.6 μm region. In an attempt to provide wavelength diversity, the Army has, in the past few years, supported the development of vibrationally Raman shifted, frequency doubled Nd:YAG lasers that provide only limited tunability within the Raman linewidth, and organic dye lasers pumped with the same source. Since the Raman shifted laser is not widely tunable, it has been excluded from consideration in this study. The Raman approach also has serious implementation problems involving the danger of a high pressure cell and the sometimes flammable or explosive nature of the chosen gas medium. Nevertheless, the Raman approach has yielded acceptable conversion efficiency and is included as a benchmark in the first-order comparison discussed below. The tunable organic dye laser has also yielded a large conversion efficiency and is not difficult to implement, although certain solute/solvent combinations are quite toxic and also flammable. In addition, due to the limited dye lifetime, the organic dye approach requires the use of a circulating flow system as well as a dye reservoir. Organic dye systems display a gradual decrease in conversion efficiency with time that is attributed to photochemical reactions resulting in the introduction of unwanted dye species into the flow system. This problem may, however, be ameliorated by the use of filters and/or a dye "bleeder" system.

In this study, we have identified three additional approaches to generating laser output in the 0.5-0.6 μm region. In Figure 1, we show all of the approaches considered to date. The first is an OPO pumped with the frequency tripled output of the Nd:YAG laser. Recently, an OPO based upon the crystal urea has been demonstrated [1] to give high conversion efficiency (20 percent at 0.53 μm) and be capable of tuning across the very wide region 0.506-0.9 μm . In addition, the crystal beta-barium borate, with perhaps even more desirable physical properties, has been demonstrated to have a similar tuning range [2].

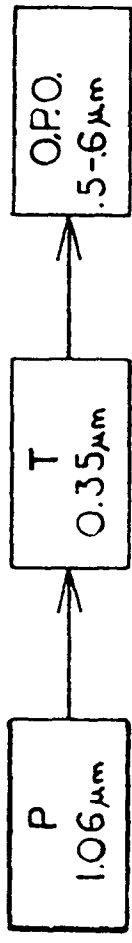
The second system we chose to study was Ti:YALO, due to the good overlap of the output fluorescence spectrum and the 0.5-0.6 μm region. This crystal has been previously grown by workers at MIT Lincoln Laboratory [3]. A recent publication [4] claimed to have provided the first demonstration of lasing however the claim is disputed. After a search of the literature and discussions with other workers in the field, we find that a paucity of data exists. While the physical properties of Ti:YALO are not expected to be significantly different from Nd:YALO, on which much previous work has been reported, the spectroscopic properties are at this time unknown. In particular, estimates of the stimulated emission cross-sections cannot be undertaken since no polarization dependent data is available. In addition, no good spectroscopic data exists for this material. Thus, it is not possible to predict whether excited-state absorption will be a problem.

LEGEND

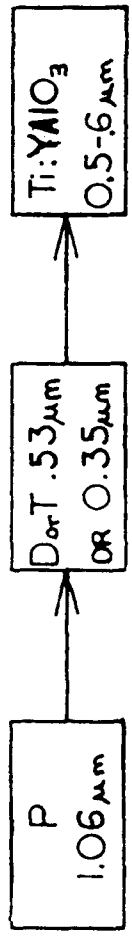
P=PUMP BEAM
D=DOUBLER
T=TRIPLER
VR=VIBRATIONAL RAMAN

FIGURE I

I. O.P.O.



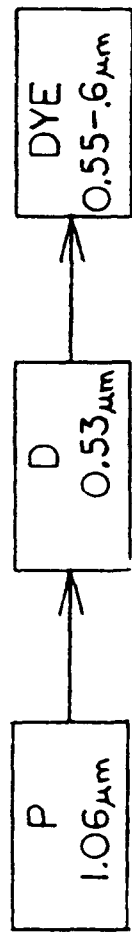
II. Ti:YAIO₃



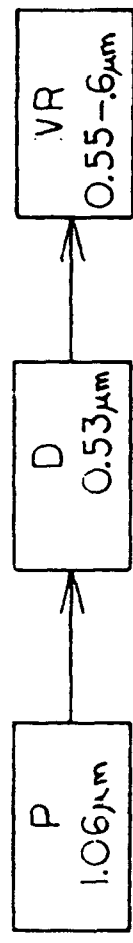
III. Ti:SAPPHIRE




IV. DYE



V. RAMAN



No.		Revisions	Date	By	LASER TECHNOLOGIES INC.
					 Scale: N.A. 16mm x 10mm (or as noted) Drawn By: M.K. Date: 9-9-78 Side 1 of 1 Checked:
TUNABLE VISIBLE LASERS					
Material:		Part Number:		Drawing No. A-0016	

For these reasons, we have dropped Ti:YALO from further consideration in this study.

The third system is Ti:Sapphire. Here, the frequency doubled output from a Nd:YAG laser is used to pump Ti:Sapphire that is lased in the 1.0-1.2 μm range and then doubled to 0.5-0.6 μm . We suspected that this system would not perform as well as the organic dye or OPO since two nonlinear conversions are required and because the Ti:Sapphire must be operated in the wing of its output profile where the stimulated emission cross-section and the extraction efficiency would be low. These suspicions have been confirmed in this Phase I study. Also shown in Figure 1 is the previously discussed organic dye laser concept.

A summary of our preliminary evaluation of the efficiency performance of the various systems considered is shown in Table 1 below. For the purposes of this comparison, we have assumed a reasonable conversion efficiency value for second harmonic generation in the range of 45-55 percent while for third harmonic generation we have assumed 60-70 percent. For the Ti:Sapphire laser we have assumed a conversion efficiency in the range of 15-50 percent based upon our previous experience that the extraction efficiency in the wings of the gain profile drops significantly. 15 percent corresponds to 1.2 μm operation. For Ti:YALO we assumed performance slightly degraded from Ti:Sapphire. Actual performance could be far worse if excited state absorption is found to be operative in this crystal. For the OPO the theoretical efficiency can be very high [1]. Here, we assume that an optimized OPO can be operated at 50 percent of the theoretical limit in the range 0.5-0.6 μm (29-35 percent). For the dye laser approach, we estimated that oscillator/amplifier configurations can convert 50 percent of the pump pulse to output near the peak of the emission wavelength. For the purposes of this initial comparison, we assumed conversion in the range of 30-55 percent in the range of interest.

In Table 1, the expected overall efficiency in the 0.5-0.6 μm range is obtained by multiplying together the efficiency factors for the various processes involved in each laser shown in Figure 1. For a comparison, where the output required in that range is assumed to be a minimum amount, the worse case efficiency for that laser may be used to determine the required Nd:YAG pump. The third column in Table 1 shows the Nd:YAG output energy/pulse to achieve a minimum output energy/pulse of 125 mJ at 0.6 μm where the efficiency is least. These preliminary results indicated that the organic dye and OPO approach are the most promising for efficiently generating tunable visible radiation. The Ti:Sapphire system is clearly not acceptable due to the low extraction efficiency at 1.2 μm , the large quantum defect, and the need for two nonlinear conversion processes. The Ti:YALO results are more attractive than Ti:Sapphire, however, not enough data is available to justify the assumed performance. It should be noted that the best performance for the dye laser and OPO approaches is similar to the fixed frequency approach of vibrational Raman scattering in methane which has achieved a conversion efficiency

of 45-55 percent from the green pump pulse, and also listed in Table 1.

Table 1: Initial Systems Efficiency Comparison

<u>System</u>	<u>Conversion Efficiency Range</u> (Nd:YAG Output → System Output)	<u>Nd:YAG</u> <u>E_s (J)</u>
Ti:Sapphire	3 - 15%	0.83 - 4.17
Ti:YALO	6 - 28%	0.45 - 2.09
OPO	17 - 25%	0.50 - 0.73
Dye	14 - 30%	0.42 - 0.89
Raman (Vibrational)	20 - 30%	0.42 - 0.63

Following this initial systems comparison, previously discussed in our Periodic Report #1, our attention was focused on further evaluating the dye laser and OPO concepts. In Section III of this Final Report we discuss each system considered during this Phase I contract in detail. Here, we discuss the specific reasons for down-selecting ultimately to the tunable dye laser concept. In Section IV we discuss the tunable dye laser approach in detail, present the modeling results obtained, and show the favored approach that offers high conversion efficiency while maintaining wide tunability and good beam quality.

II. Executive Summary of Phase I:

The ultimate goal of this Phase I feasibility study was to choose, from amongst a number of candidate laser systems, an approach to producing a tunable visible laser that combines the attributes of good conversion efficiency from Nd:YAG output to tunable laser output, tunability in the 0.5-0.6 micron region, and good beam quality. As discussed in more detail below, this study has produced a number of recommendations, the most important of which are:

- (1) An improved organic dye laser incorporating an oscillator/amplifier approach can provide optimum conversion efficiency.
- (2) A double-passed amplifier incorporating optical phase conjugation via Stimulated Brillouin Scattering can result in near-diffraction-limited beam quality. LTA has generated a unique design (to be patented) for achieving this while maintaining system compactness.
- (3) At the average power levels needed for present day US Army applications (typically 30 watts), the use of a phase-conjugated double pass straight-through amplifier is preferred compared to a zig-zag or slab amplifier geometry due to the simplicity of the approach and experimentally demonstrated aberration compensation.
- (4) The OPO approach may offer the best long-term solution to

providing an all solid-state laser source operating in the 0.5-0.6 micron region and beyond.

In Sections III and IV which follow, we discuss each of these conclusions in detail.

III. Systems Evaluation:

In this section of this Phase I Final Report, we separately discuss each of the different laser systems considered.

(a) Ti:YALO Laser

YALO is a clear crystal possessing the orthorhombic structure. The crystal is biaxial. There are three distinct crystal axes (a,b,c), each of which displays optical and physical properties distinct from the others. The only known believable absorption and fluorescence spectra for this material were published recently, although it is not clear which crystal axis the data was taken along [5]. The only other information concerning this material was obtained from a Czechoslovakian journal [4]. Crude absorption data is shown, and the lifetime was measured to be in the range of 12-14 μ sec, or about four times that of Ti:Sapphire. In order to fully characterize this promising material, it is necessary to obtain absorption and fluorescence data along the crystal axes. From such data and the fluorescence lifetime of the material, it is straightforward to obtain the stimulated-emission cross-section as a function of wavelength as has been done recently for Ti:Sapphire [6].

In order to correctly predict and optimize the performance of laser oscillators and oscillator/amplifier systems, it is necessary to provide absorption and cross-section data as well as the passive loss expected. Attempts to estimate the value of the emission cross-sections based upon a comparison to Ti:Sapphire will not be fruitful because of the fact that Sapphire has a rhombohedral structure (uniaxial) and thus, the local field will be different. For this reason, it is not possible to say with certainty that excited-state absorption will not be a problem in Ti:YALO since it is not exhibited in Ti:Sapphire. Due to the scarcity of data concerning this material, we eliminated it early in this study. Discussions with one crystal manufacturer [8] have led us to conclude that Ti:YALO crystals suitable for spectroscopic investigation will be available in about a year, and could be the subject of a joint SBIR program.

(b) Ti:Sapphire Laser

Ti:Sapphire, a material with an unusually wide tuning range (0.65-1.2 μ m), has undergone intensive development during the past few years. Due to a short fluorescence lifetime, this material is most efficiently pumped by use of a short Q-switched pulse of green (0.532 μ m) light obtained from a doubled Nd:YAG laser. A plot of the emission cross-sections for this material is shown in Figure 2. The peak emission cross-section is now agreed

TI:AL₂O₃
EMISSION CROSS-SECTION

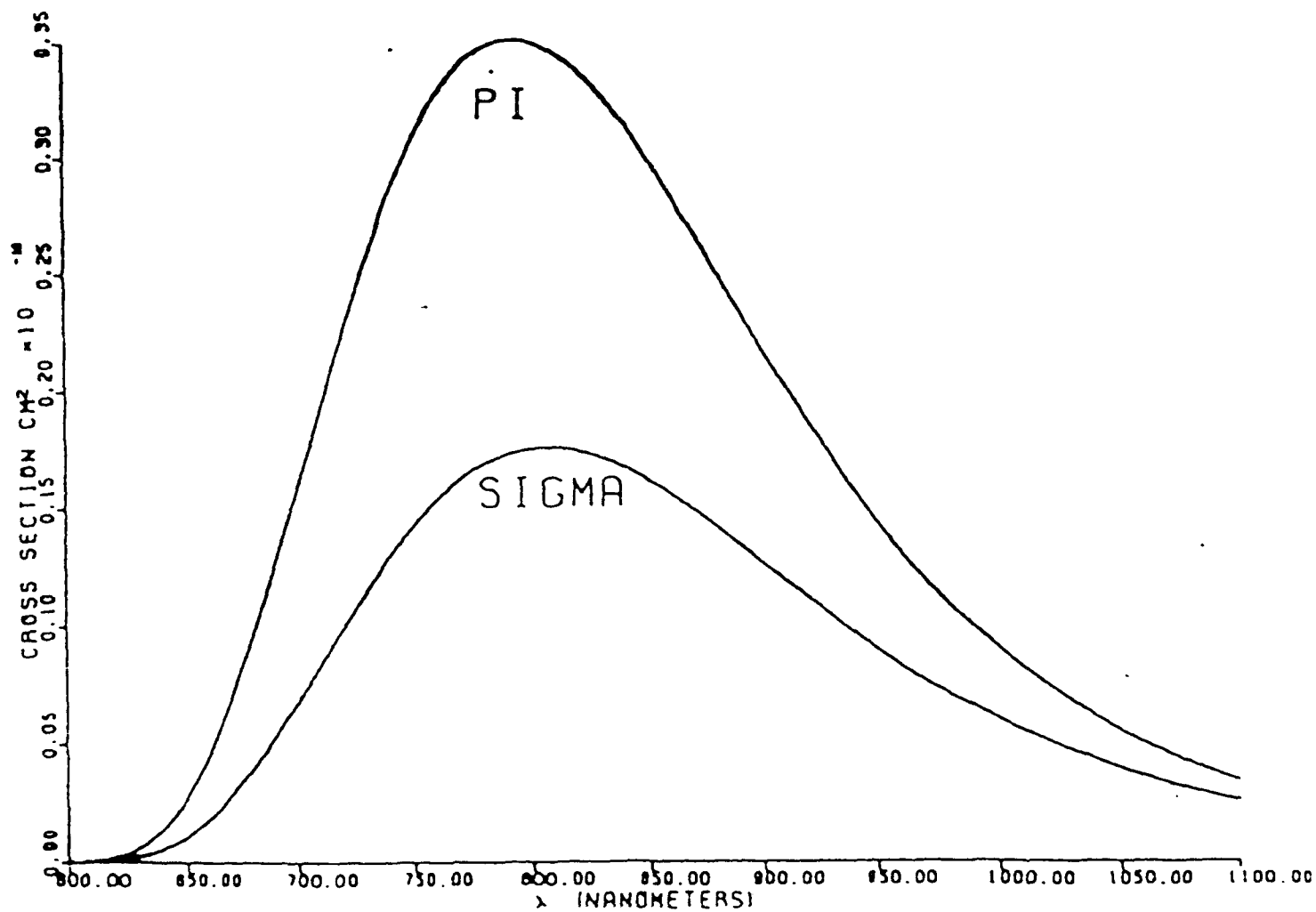


FIGURE 2

to be in the vicinity of $3.5 \times 10^{-17} \text{ cm}^2$ [7] at the peak wavelength of $0.79 \text{ }\mu\text{m}$ for the sigma polarization. The plots shown in Figure 2 were obtained by scaling the published values of the peak cross-sections [6] and using the Poisson distribution. Extensive work on the Ti:Sapphire system has shown that excited-state absorption in this material is absent, demonstrating efficient laser action.

In order to create a visible tunable laser with Ti:Sapphire it is necessary to operate the laser in the wing of the emission band between 1.1 and $1.2 \text{ }\mu\text{m}$. As shown in Figure 2, the emission cross-section in that region is reduced by a factor of 7-8 as compared to the peak wavelength. This is problematical for two reasons. First, the reduced cross-section will lead to lower extraction efficiencies as shown below. Second, due to parasitic oscillations and amplified spontaneous emission (ASE), the laser cannot be pumped harder to create a larger inversion density since limits to that density are determined by the peak gain, not the gain in the 1.1 - $1.2 \text{ }\mu\text{m}$ region. An additional factor to consider is that the large quantum defect between the pump and emission wavelengths also leads to a lower efficiency. The maximum theoretical extraction efficiency in the 1.1 - $1.2 \text{ }\mu\text{m}$ region can easily be calculated to be between 48-44 percent respectively. By contrast, green pumped lasers ($0.532 \text{ }\mu\text{m}$) operating in the 0.55 - $0.6 \text{ }\mu\text{m}$ region have maximum theoretical quantum efficiencies in the range of 97-89 percent, or about double that obtainable with Ti:Sapphire.

We have completed an analysis of a $0.532 \text{ }\mu\text{m}$ pumped Ti:Sapphire laser by use of a quasi-cw analysis based upon a Rigrod formulation. This approach has been used previously to model the performance of Ti:Sapphire oscillators and found to be very accurate [8]. While this approach will not provide any details concerning the output pulsewidth or the system dynamics, it will allow us to determine the size of the green pump or the Nd:YAG laser needed to provide a given output energy/pulse in the 0.5 - $0.6 \text{ }\mu\text{m}$ region. The overall extraction efficiency, η_o , of the Ti:Sapphire oscillator can be written:

$$\eta_o = \left[\frac{1}{\alpha_l l - \ln(R)} - \frac{1}{g_o l} \right] \left[\frac{1-R}{1+R} \right] \left[\frac{\lambda_p}{\lambda_l} \right] (1 - e^{-\alpha l}) \quad (1)$$

where α is the pump absorption coefficient, λ_p and λ_l the pump and laser wavelengths, R the Ti:Sapphire output coupler reflectivity, α_l the laser passive loss coefficient, l the crystal length, and $g_o l$ the gain-length product given by:

$$g_o l = \alpha_o J_s \left[\frac{\lambda_p}{\lambda_l} \right] (1 - e^{-\alpha l}) \quad (2)$$

Here, α_o is the specific gain coefficient and J_s the maximum safe operating pump fluence incident upon the Ti:Sapphire crystal which we assume is end pumped. Note that in this model we assume

that the absorbed pump energy is uniformly distributed along the pumped crystal. For a safe operating fluence of 3.5 J/cm^2 and assuming that all the pump fluence is absorbed, the value of $g \cdot l$ obtained from (2) is about 3.

From (1), we can see that two optimizations are involved in maximizing the extraction efficiency. First, for every Ti doping level, an optimum length exists. Choosing a longer length results in too much loss from the passive loss-length product while a shorter length would result in too little absorption. Furthermore, for each length chosen there exists an optimum value of the outcoupler reflectivity R . This twofold optimization can easily be achieved by use of a computer. We have completed such optimizations for Ti concentrations varying from $1\text{--}5 \times 10^{19} \text{ ions/cm}^3$, and for the wavelengths 0.8, 1.0, and 1.1 μm . In Figures 3-5 we show plots of the extraction efficiency for each of the three wavelengths and for a concentration of $5 \times 10^{19} \text{ ions/cm}^3$ as a function of outcoupler reflectivity and crystal length.

It can be seen that the maximum extraction efficiencies at 0.8, 1.0, and 1.1 μm are 44, 29, and 21 percent, respectively. The optimum reflectivity and crystal length may be more easily visualized using the accompanying contour plots shown in Figures 6-8. Note that these maximum extraction efficiencies compare to the theoretical extraction efficiencies of 67, 53, and 48 percent, respectively. We have found that optimized extraction efficiencies more closely approach the theoretical values when a very large Ti concentration is assumed ($10 \times 10^{19} \text{ ions/cm}^3$) and the loss at the lasing wavelength is very low (0.01 percent). An example of this is shown in Figure 9 where, for 0.8 μm , the extraction efficiency is over 59 percent. It is difficult to obtain Ti:Sapphire crystals with Ti dopings over $5 \times 10^{19} \text{ ions/cm}^3$ with good optical quality. However, as the technology improves we can expect that extraction efficiencies close to the theoretical limit may be approached.

One can observe from Figures 3-8 that as we operate the laser further out in the wing of the Ti emission band the extraction efficiency drops significantly, as expected. The worst case, of course, is at 1.2 μm where only 11 percent of the pump energy is converted to output energy. Suppose that approximately 125 mJ of output energy is required at the 0.6 μm wavelength. If we assume a reasonable second harmonic conversion efficiency in the range of 45-55 percent, then 227-278 mJ of Ti:Sapphire output is required. With 11 percent extraction efficiency, this means that 2.12-2.60 J/pulse of green 0.53 μm output is required, or that the fundamental Nd:YAG laser must provide an output of 3.9-5.8 J/pulse. This requirement is almost four times that needed for alternative approaches such as the organic dye laser and the OPO.

Since these optimizations of Ti:Sapphire have yielded such large values for the required Nd:YAG pump energy/pulse (or equivalently the transfer efficiency from Nd:YAG to Ti:Sapphire output is so low), this option was dropped from further investigation in this study.

Ti:Al₂O₃ OVERALL EXTRACTION EFFICIENCY

λ = 0.800 μm
 σ (0.800 μm) = $3.49 \times 10^{-17} \text{ cm}^2$
 $[Ti(\text{ions/cc})]$ = $5.00 \times 10^{17} \text{ ions/cm}^3$
 J_0 = 3.50 Joules/cm²
 α = 0.075 cm⁻¹
 $\eta_{\text{e}}(\text{max})$ = 0.4399

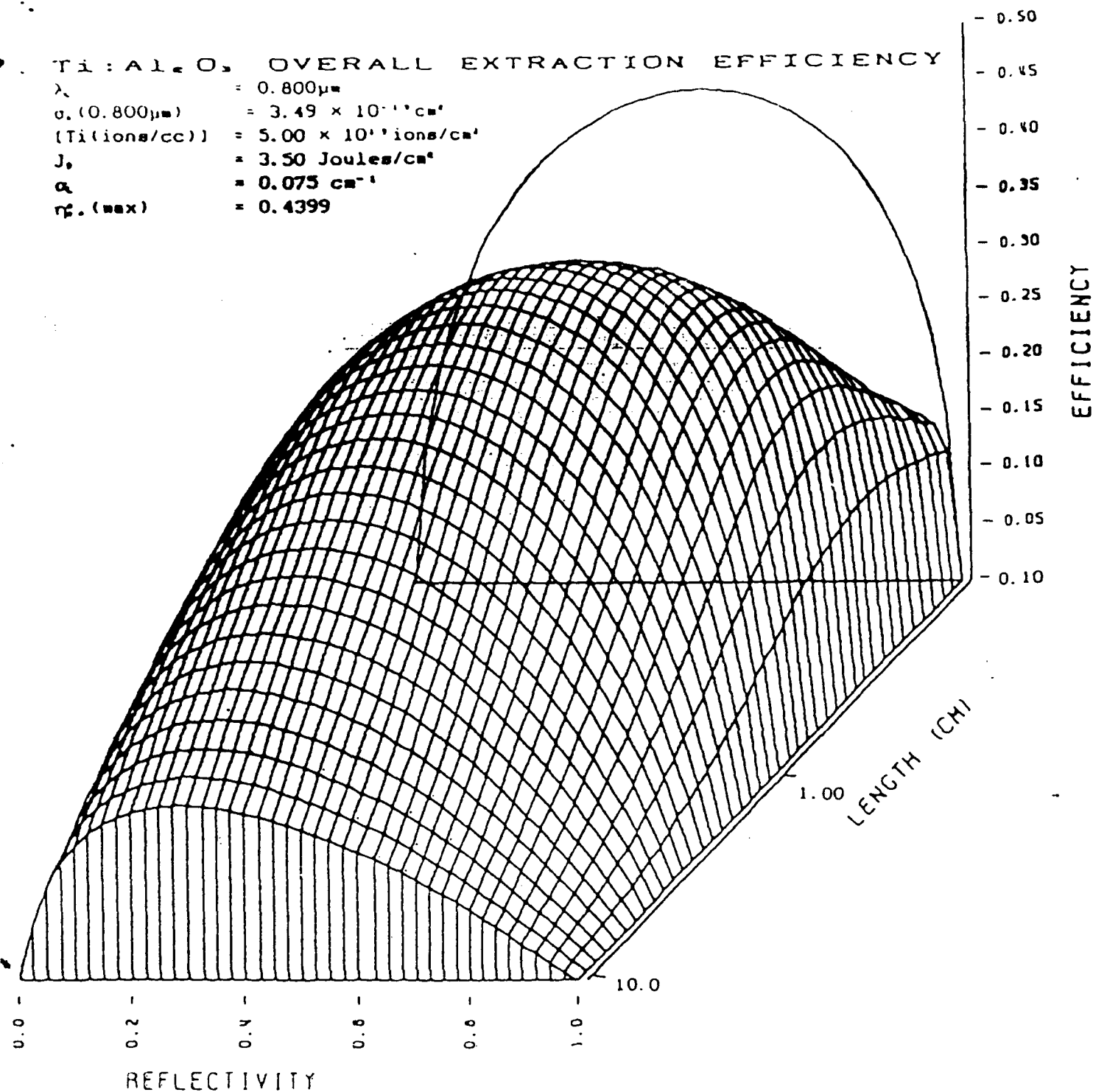


FIGURE 3

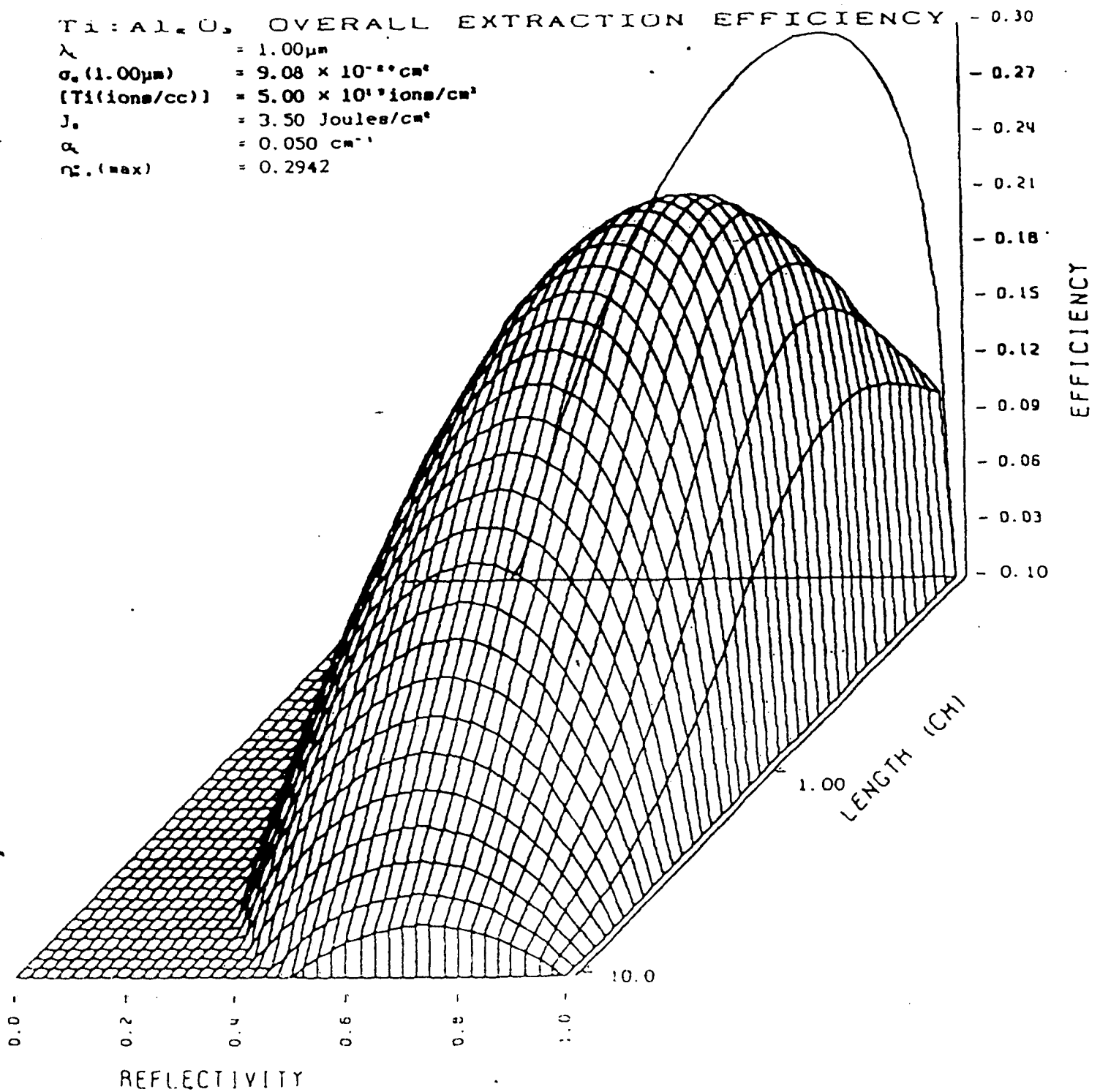


FIGURE 4

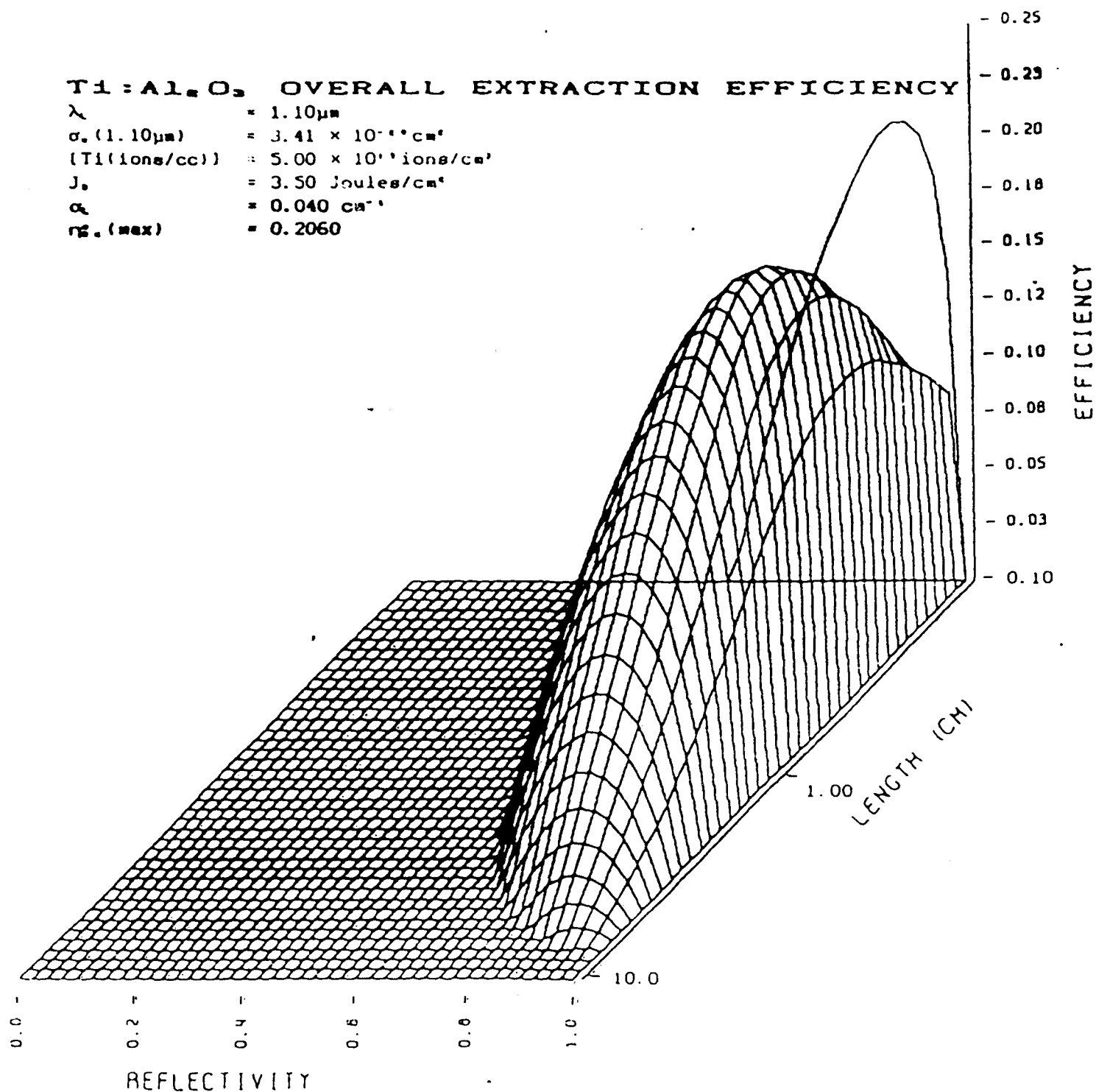


FIGURE 5

T1:Al₂O₃, OVERALL EXTRACTION EFFICIENCY
 λ = 800nm
 $q_{\lambda}(800\text{nm})$ = $3.49 \times 10^{-11} \text{ cm}^2$
 $[T1(\text{ions/cc})]$ = $3.00 \times 10^{17} \text{ ions/cc}$
 J_0 = 3.30 Joules/cm²
 ρ_{λ} = 0.075 cm⁻¹
 $\eta_{\lambda}(\text{max})$ = 0.4399

PLOT KEY

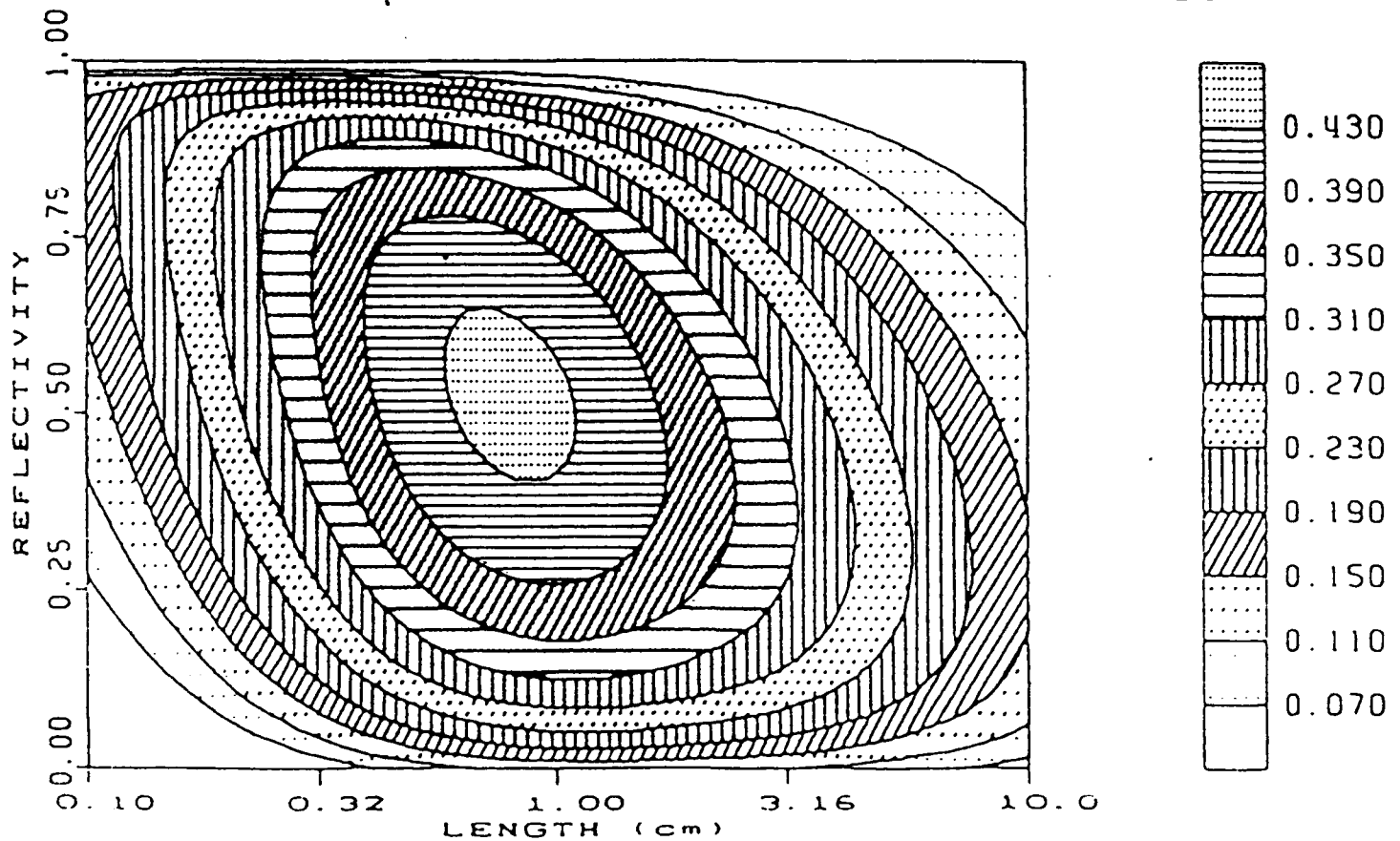


FIGURE 6

Ti:Al₂O₃ OVERALL EXTRACTION EFFICIENCY
 λ = 1.00 μm
 α (1.00 μm) = $9.08 \times 10^{-4} \text{ cm}^{-1}$
 $[Ti(\text{ions/cc})]$ = $3.00 \times 10^{17} \text{ ions/cc}$
 η = 3.50 Joules/cm²
 η_{max} = 0.050 cm⁻¹
 $\eta_{\text{max}} (\text{max})$ = 0.2942

EFFICIENCY

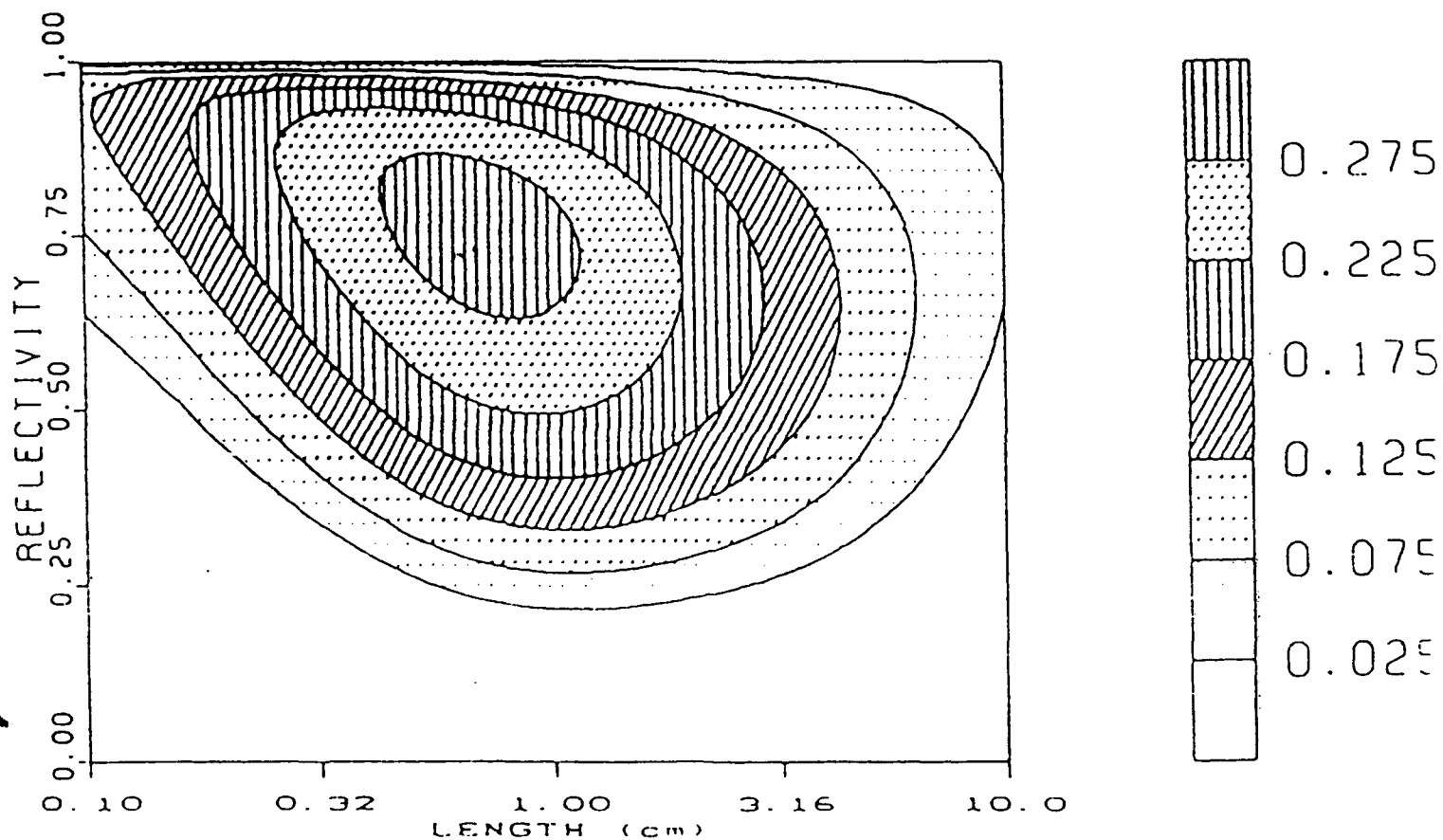


FIGURE 7

T1:Al.O, OVERALL EXTRACTION EFFICIENCY
 λ = 1.10 μm
 q_1 (1.10 μm) = $3.41 \times 10^{-10} \text{ cm}^2$
 $[T1(10\text{ns}/\text{cc})]$ = $5.00 \times 10^{10} \text{ ions/cc}$
 J_0 = 3.50 Joules/ cm^2
 q_0 = 0.040 cm^{-1}
 η_{max} (max) = 0.2060

EFFICIENCY

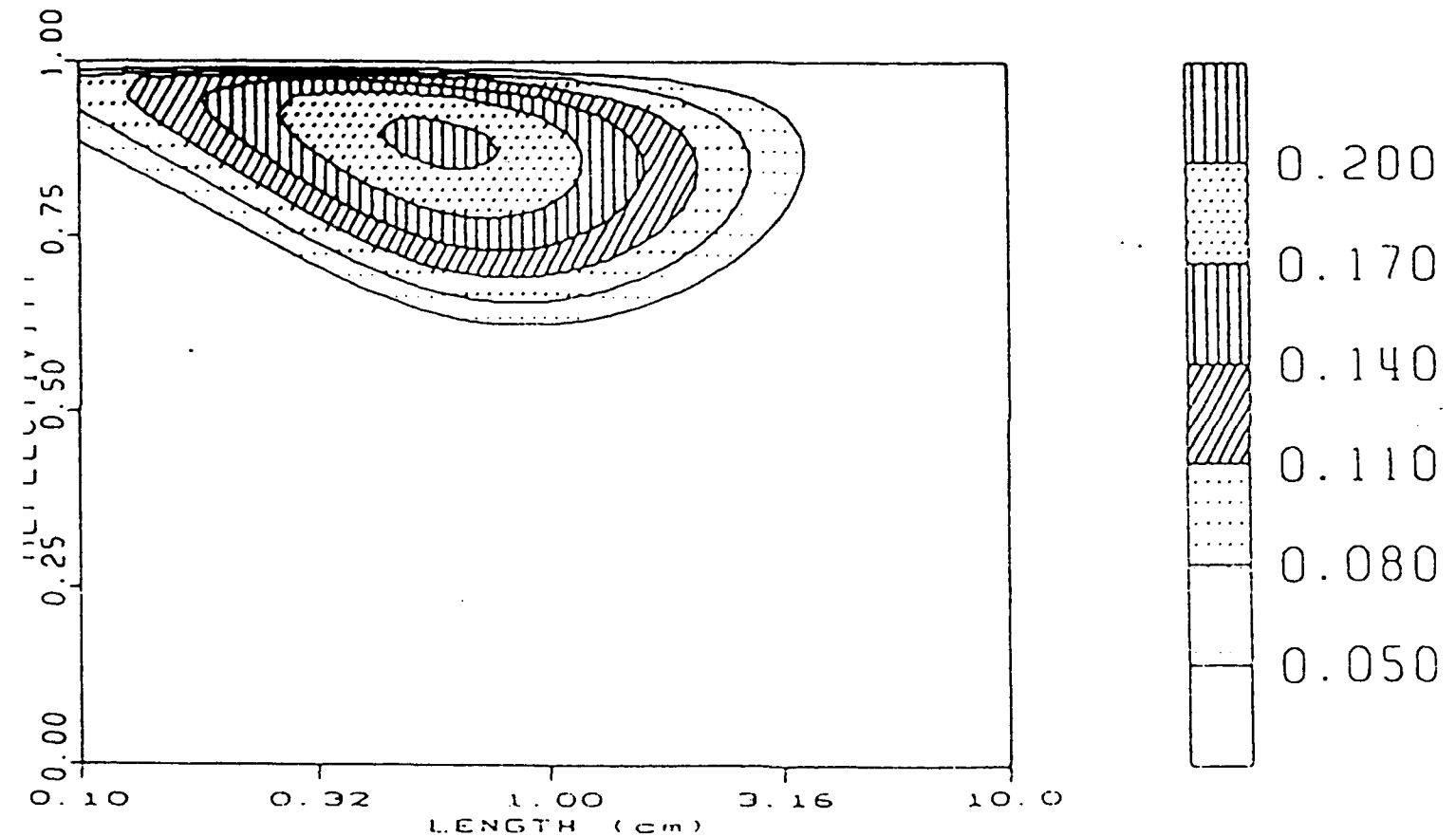


FIGURE 8

Ti:Al₂O₃ OVERALL EXTRACTION EFFICIENCY

λ = 0.800 μm
 $\sigma_c(0.800 \mu\text{m})$ = $3.49 \times 10^{-19} \text{ cm}^2$
 (Ti ions/cc) = $10.00 \times 10^{19} \text{ ions/cm}^3$
 J_s = 3.50 Joules/cm²
 α = 0.010 cm⁻¹
 $\eta_{\text{ex}}(\text{max})$ = 0.5929

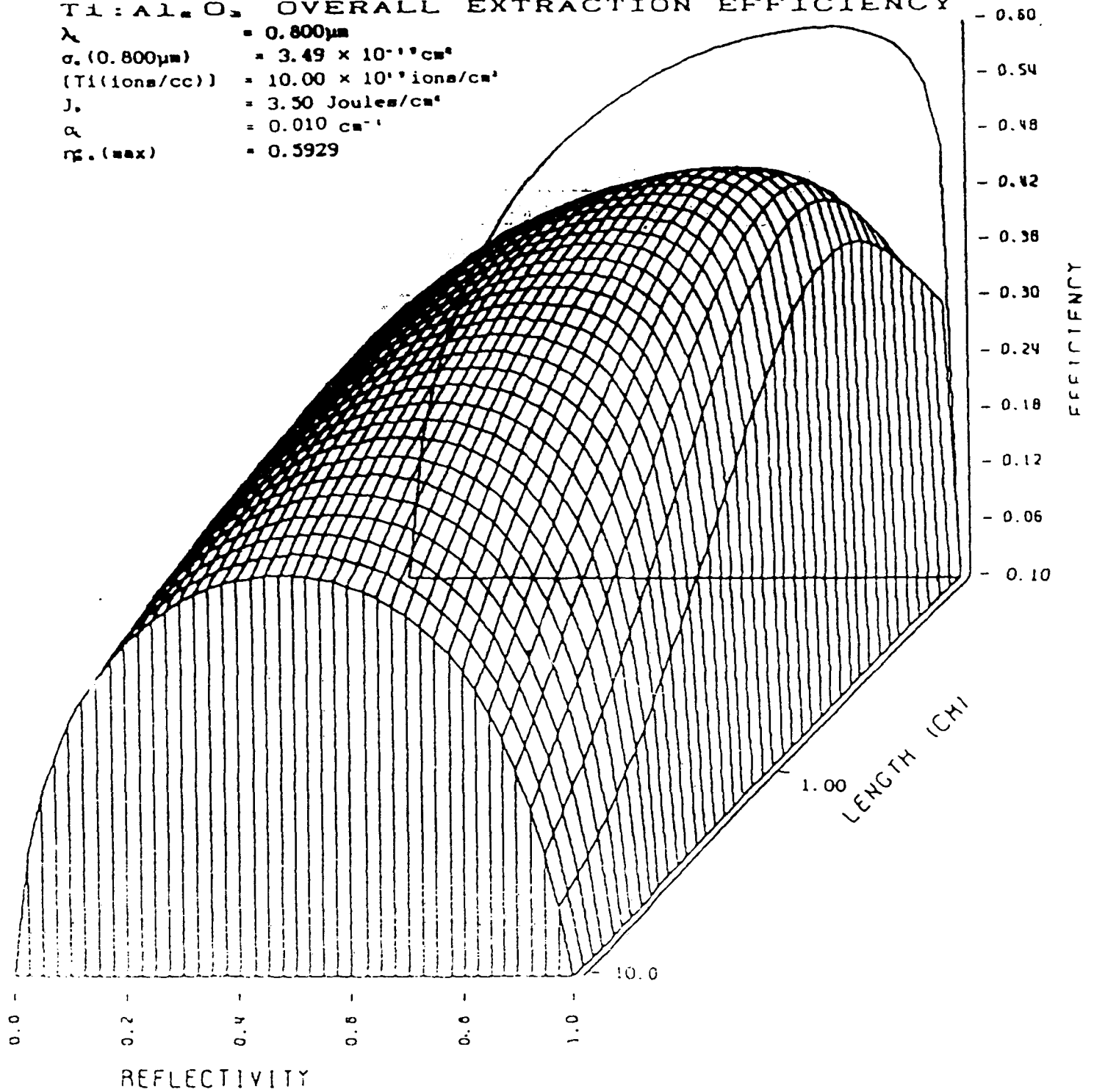


FIGURE 9

(c) Optical Parametric Oscillator

The OPO has been widely recognized for some time to have the potential for widely tunable operation with good efficiency [9]. Progress in this area has lagged until recently because of the lack of suitable crystalline materials. This situation has changed only in the past few years with the investigation of new OPO materials, in particular, the crystal urea at Cornell [10, 11] and beta-barium borate in The Peoples Republic of China [2]. In a recent article [11] substantial progress was reported in the operation of a urea OPO. The urea crystal was pumped by the third harmonic of a Q-switched Nd:YAG laser. Tunable output was achieved from 0.506-0.9 μm . Urea may be phase-matched across the wide spectral region 0.5-1.225 μm . The region from 0.5-0.6 μm is of particular interest since the theoretical conversion efficiency is very high (59-71 percent). In the work reported in [11], a conversion efficiency of 20 percent was achieved at 0.53 μm in an unoptimized arrangement. A potential problem with this material has been the rather low damage threshold (40 MW/cm²). By contrast, the newer material beta-barium borate (BBO) has displayed a very large damage threshold (13.5 GW/cm²) [2]. BBO can also be used for third harmonic generation, and can yield a conversion efficiency of 60-70% for the pulse parameters considered here. Due to the much lower damage threshold of KD*P, our simulations show a disappointingly low conversion for the same pulse parameters. In addition, the crystal BBO has an extraordinarily large tuning range (0.4-2.0 μm) when pumped by a tripled Nd:YAG laser and good transmission from 0.2-2.6 μm . The output wavelength range can be increased further by frequency doubling the OPO output down to 0.2 μm .

Parametric oscillation is a nonlinear process in which the incident frequency ω_i is converted to two coherent lower frequency beams with frequencies ω_s (signal) and ω_i (idler), and so, is the inverse process to sum frequency generation. Placing a nonlinear crystal in a cavity will, at some threshold value, result in oscillation at both frequencies. In practice, oscillating both frequencies (doubly resonant operation) leads to significant amplitude stability problems [9], thus resonance at one frequency is preferred. This is achieved by use of high reflectivity mirrors at one frequency and low reflectivity at the other. The OPO output wavelength is normally tuned by changing the angle of the crystal with respect to the optical axis. The ray internal angle is changed, resulting in a different wavelength being optimally phase-matched.

The coupled equations describing parametric amplification are well known, and in fact are identical to those describing sum frequency generation. Thus, one set of coupled equations can be used to describe second and third harmonic generation and parametric amplification. The paraxial equation, used to describe beam propagation in free-space or in linear and nonlinear media, is given by:

$$2ik \frac{\delta E}{\delta z} = [\nabla_1^2 + k_0^2(n^2-1) - ik\alpha_1 + f(E)] E \quad (3)$$

Here, the propagation of a field E in the $+z$ direction is described. The first term on the right hand side describes diffraction, the second, phase distortion (for example from thermal effects), the third, linear absorption, and the last can account for nonlinear effects or two beam coupling as one has, for example, in second or third harmonic generation or parametric amplification. For the case of parametric amplification, (3) becomes (A_1 is the pump wave):

$$2ik \frac{dA_1}{dz} = [\nabla_1^2 + k_0^2(n^2-1) - ik\alpha_1 + kgA_2^* e^{-i\Delta kz}] A_1 \quad (4)$$

for the "signal" wave A_1 to be amplified in the OPO and A_2 the "idler" wave amplitude. Here, Δk is given by:

$$\Delta k = k_3 - (k_1 + k_2) \quad (5)$$

and g by:

$$g = 2 \left[\frac{\mu_0}{\epsilon_0} \left(\frac{\omega_1 \omega_2}{n_1 n_2} \right) \right]^{1/2} d_{eff} A_2 \quad (6)$$

It is significant that in an OPO, phase matching can be satisfied only in the direction of the pump wave. Thus, amplification takes place only once in each round trip. For this reason, if an OPO is to be used exclusively, it should be constructed in a ring oscillator configuration, with the circulating wave traveling in the pump wave propagation direction in the nonlinear crystal. This arrangement assures that the minimum passive losses occur, maximizing the OPO conversion efficiency.

Most OPO experiments reported to date have used a frequency tripled Nd:Host laser as a source. The difficulty with this is that in the spectral region of interest, 0.5-0.6 microns, the maximum conversion (quantum) efficiency can only be 0.71-0.59, respectively. To achieve an efficiency comparable to the organic dye laser, the OPO must be pumped with a frequency doubled Nd:Host source. This may be achieved using the crystal KTP for example. In [12], phase matching curves for a frequency doubled Nd:YLF laser are presented. Unfortunately, phase matching at wavelengths much less than 0.6 microns is not possible using this laser source. Similar phase matching curves for BBO are reported in [2] for the third harmonic of Nd:YAG, but not the second harmonic.

Our assessment of the OPO concept is that it may offer the best performance in the long term, but that the present state-of-the-art is not sufficient to compete with the organic dye laser. The

never high efficiency crystals have not reached a mature state. A sufficient quantity of large crystals with good optical quality is not currently available. Another difficulty with the OPO concept is that if a strictly oscillator approach is used, it will not be as efficient as the dye laser concept discussed below. The efficiency of any oscillator is very sensitive to the value of the intra-cavity losses, since usually a large number of round trips are involved. This is precisely the reason why a dye laser oscillator/amplifier configuration is more efficient than an oscillator only. In the optimum configuration, only enough pump energy is provided to the oscillator to provide enough fluence to completely saturate the following single or double passed amplifier. The oscillator does not need to be particularly efficient. Experiments in which an OPO is followed by an amplifier (traveling wave) have not yet been reported. It is likely, however, that the most efficient system will involve using both an OPO followed by an optical parametric amplifier (OPA). To implement this concept, larger nonlinear crystals than now exist are required.

Another important point is that if an all oscillator approach is used for either the organic dye or OPO approaches, it is difficult to produce an output beam near the diffraction limit. While various techniques have been investigated for using OPC as an integral part of an oscillator [13] in order to correct thermally induced aberrations, such techniques are usually only partially successful and greatly complicate the device implementation. If, however, only a small amount of the pump energy is deposited in the oscillator, near diffraction-limited operation is achieved. The remaining large amount of the pump is then used to drive a following amplifier stage. If a double passed extraction scheme is used, it is then possible to almost completely remove any thermal aberrations by using a phase-conjugation cell as the "mirror" for the double pass. This is the approach we have taken in the dye laser design discussed in the next Section of this Final Report. The same system architecture can be used for an OPO followed by a double passed OPA. While amplification can take place only on one of the amplifier traverses (phase matching and amplification can take place only in the direction of the pump beam), double passing the crystal will remove thermally induced aberrations.

To summarize, it is our opinion that the OPO/OPA concept will eventually replace the organic dye laser because of its all solid-state nature, wide tunability, and potential efficiency. Much additional work involving the growth of large optical quality crystals remains for this concept to become a reality. In addition, experimental work is needed to validate the OPO/OPA concept.

(d) Tunable Dye Laser

(1) Tunable Dye Lasers: General

The tunable dye laser has undergone intensive development since its first demonstration in 1966. Several commercial laser manufacturers offer frequency doubled or tripled Nd:YAG pumped dye laser systems that operate across the entire visible and near ultraviolet regions. Early investigations of laser pumped dye lasers were concerned with the generation of ultra-narrowband radiation ($<10^{-4}\text{nm}$) in various oscillator configurations pumped with N_2 lasers [14]. Here, we are most interested in frequency doubled Nd:YAG laser pumped dye lasers. In order to maintain high frequency doubling conversion efficiency, high peak power Q-switched pulses must be used. Single-shot or low repetition rate conversion efficiencies slightly greater than 60 percent have previously been demonstrated with high beam quality (e.g. phase-conjugated) in the multi-tens of watts average power regime, while values in the range of 40-50% are typical of non-phase-conjugated lasers. These numbers apply to Q-switched Nd:YAG lasers producing typically 250 mJ/pulse of $1.06\text{ }\mu\text{m}$ energy with a pulsewidth (FWHM) of typically 5-10ns.

The dye laser is unique in that fluorescence lifetimes of typical organic dyes are in the nanosecond regime. As an example we mention that the lifetime of the well-known dye Rhodamine 6G is only about 6 ns [14]. Since the lifetime is comparable to the duration of the Q-switched pumping pulse, a laser oscillator will have a finite number of round trips and a true mode structure is never established. In fact, a short pulse dye laser oscillator is really a superfluorescence or ASE based device whose brightness is usually less than that obtainable with a longer fluorescence lifetime gain medium.

A schematic of the energy level diagram of a dye laser molecule is shown in Figure 10, and consists of a single and a triplet manifold. Excitation of the molecule is via the ground singlet state S_0 to the first singlet manifold S_1 . Relaxation from the upper state manifold can occur via a radiationless transition to the first triplet manifold T_1 , by fluorescence decay to the ground state, or by stimulated emission to the ground state. Because the transition $S_1 \rightarrow T_1$ is forbidden, the process is usually slow. For Q-switched lasers it may be entirely ignored, although for CW lasers the process is important [14]. In Figure 11, we show the absorption cross-section σ_a , emission cross-section σ_e , and triplet cross-section σ_t as a function of wavelength for a 10^{-4} M solution of Rhodamine 6G in water. $E(\lambda)$ is the fluorescence intensity, related to the emission cross-section through the relationship [14]:

$$\sigma_e(\lambda) = \frac{\eta E(\lambda) \lambda^4}{8 \pi n^2 c \tau} \quad (7)$$

Here, n is the index of refraction, η the quantum efficiency, and

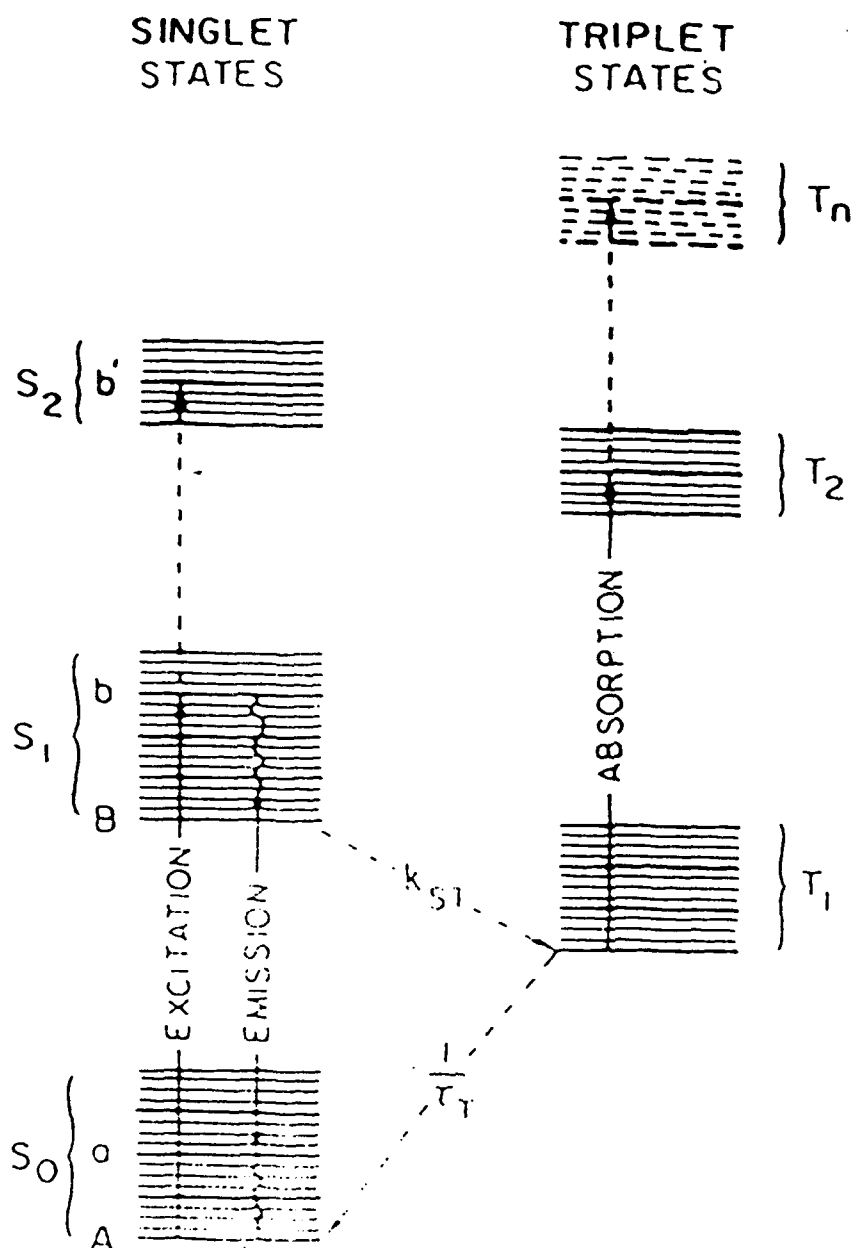


FIGURE 10

Continuous-Wave Dye Lasers

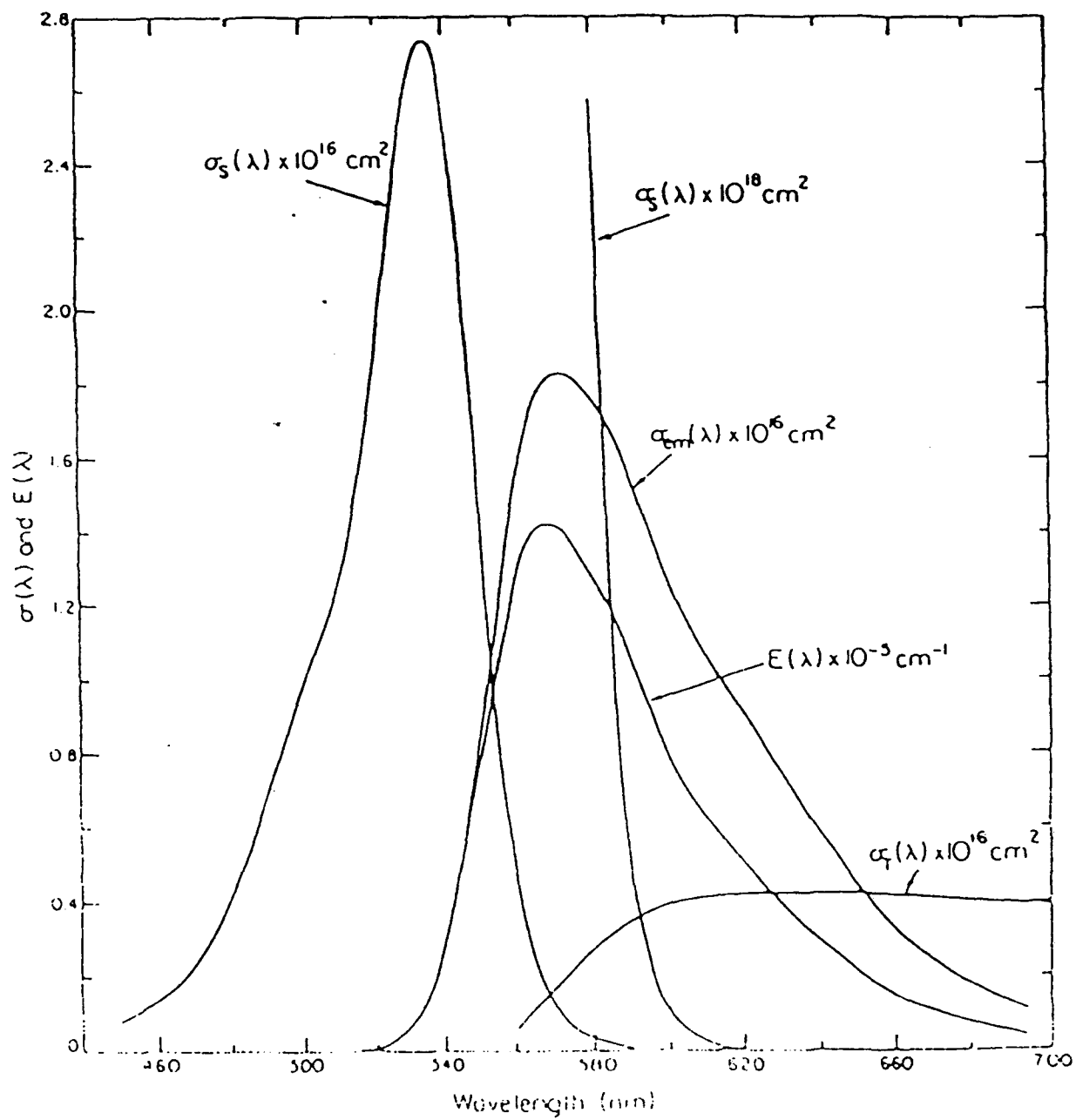


FIGURE 11

λ the wavelength. The absorption of pump radiation intensity I_p with distance z is described by the relationship:

$$\frac{dI_p}{dz} = -n_0 \sigma_0 I_p \quad (8)$$

where n_0 is the ground state population and σ_0 the singlet absorption cross-section. The laser intensity I_L is amplified according to the equation:

$$\frac{dI_L}{dz} = (\sigma_E n_E - \sigma_0 n_L) I_L \quad (9)$$

n_E and n_L are the upper and lower level ion densities and σ_E the emission cross-section. If λ_0 and λ_L are the pump and laser wavelengths, respectively, the time evolution of the upper laser level population density can then be written:

$$\frac{dn_E}{dt} = \frac{\sigma_0 n_0 I_p \lambda_0}{hc} - \frac{n_E}{\tau} - \frac{\sigma_E n_E I_L \lambda_L}{hc} \quad (10)$$

The first term on the right hand side of (10) represents the rate of arrival of ions in the upper laser level, the second, fluorescence decay with time constant τ , and the third, removal of ions via stimulated emission. The last term arises due to the singlet absorption of laser photons. Note that due to the short fluorescence decay time of dyes, it cannot be neglected in this analysis as is often the case with laser pumped lasers with lifetimes of hundreds of microseconds. An additional relationship needed in the analysis is the conservation of ions, giving:

$$n_0 + n_E = n_0 \quad (11)$$

where n_0 is the total ion density.

Equations (7-11) represent those physical relationships needed to accurately describe the operation of Q-switched pumped dye lasers in which triplet state effects are minimal. The use of these relationships in our oscillator/amplifier simulation code is described in Section IV of this Final Report.

(2) Thermal Effects in Dye Lasers

Another subject of interest in connection with dye lasers is the obtainable beam quality. Liquid solutions are known [15] to display very large changes in index of refraction with temperature. Furthermore, relaxation within a manifold via multi-phonon transitions takes place on a picosecond time scale. Because of this, even short pulse Q-switched dye lasers are subject to self-induced thermal aberrations. Note that this limitation cannot be removed by dye circulation since, during a pulse, the dye medium is essentially "frozen" in place. The deposition of heat in the

pumped dye laser volume follows the radial distribution of pump fluence which is often complicated. Even in the ideal case in which the pump pulse is a transverse Gaussian, the instantaneous heat profile will be the same and thus uncorrectable with conventional optical elements. While some correction may be possible in an RMS sense, it is clear that transverse temperature and, therefore, index of refraction gradients are formed and a degradation in beam quality occurs.

We have completed an analysis of this effect. The following equation for a Gaussian beam of $1/e$ radius r_0 estimates the thermal distortion $\Delta\phi$ in terms of the incident fluence J , the pump and laser wavelengths λ_p and λ_l , the density ρ , specific heat c , and the quantity $\beta = dn/dT$:

$$\Delta\phi(\lambda) = \frac{2\pi J}{\lambda_l} \left[1 - \frac{\lambda_p}{\lambda_l} \right] \left[\frac{\beta}{\rho c} \right] e^{-(r/r_0)^2} \quad (12)$$

A standard way of evaluating beam quality for small aberrations is the use of Strehl's ratio S [16] which represents the peak intensity of an aberrated beam in the far field divided by the peak intensity of a diffraction limited beam at the same location. S is formally given by:

$$S = 1 - \left[\frac{2\pi}{\lambda} \right]^2 (\Delta\phi)^2 \quad (13)$$

where $(\Delta\phi)^2$ is the "mean square deformation" of the wave front. We have evaluated S for the case of an end pumped dye laser and obtain the following expression:

$$S = 1 - \left[\frac{K r_0}{2a} \right]^2 (1 - 2(r_0/a)^2) \quad (14)$$

a is the Gaussian radius at which the intensity has reached 10^{-3} of its peak intensity and K is a constant. In Figure 12, we show an evaluation of the Strehl ratio as a function of the incident green pump fluence in the range of 0-4 J/cm² for a methanol solvent. The Strehl ratio may also be related to another measure of beam quality, the number of times diffraction-limited N [14], through the relationship:

$$N = S^{-1/2} \quad (15)$$

N has also been plotted in Figure 12. It can be seen that as the input pump fluence increases, the Strehl ratio decreases while N increases.

This decrease of beam quality as the pump fluence increases is a single shot effect. Average power effects can generally be overcome by circulating or flowing the solution. For laser systems involved in tactical or scientific applications, the

GAUSSIAN PUMP BEAM
DYE/METHANOL SOLUTION
 $\left(\frac{a}{r_0}\right) = 6.91$

$$\lambda_p = 0.53 \mu\text{m}$$

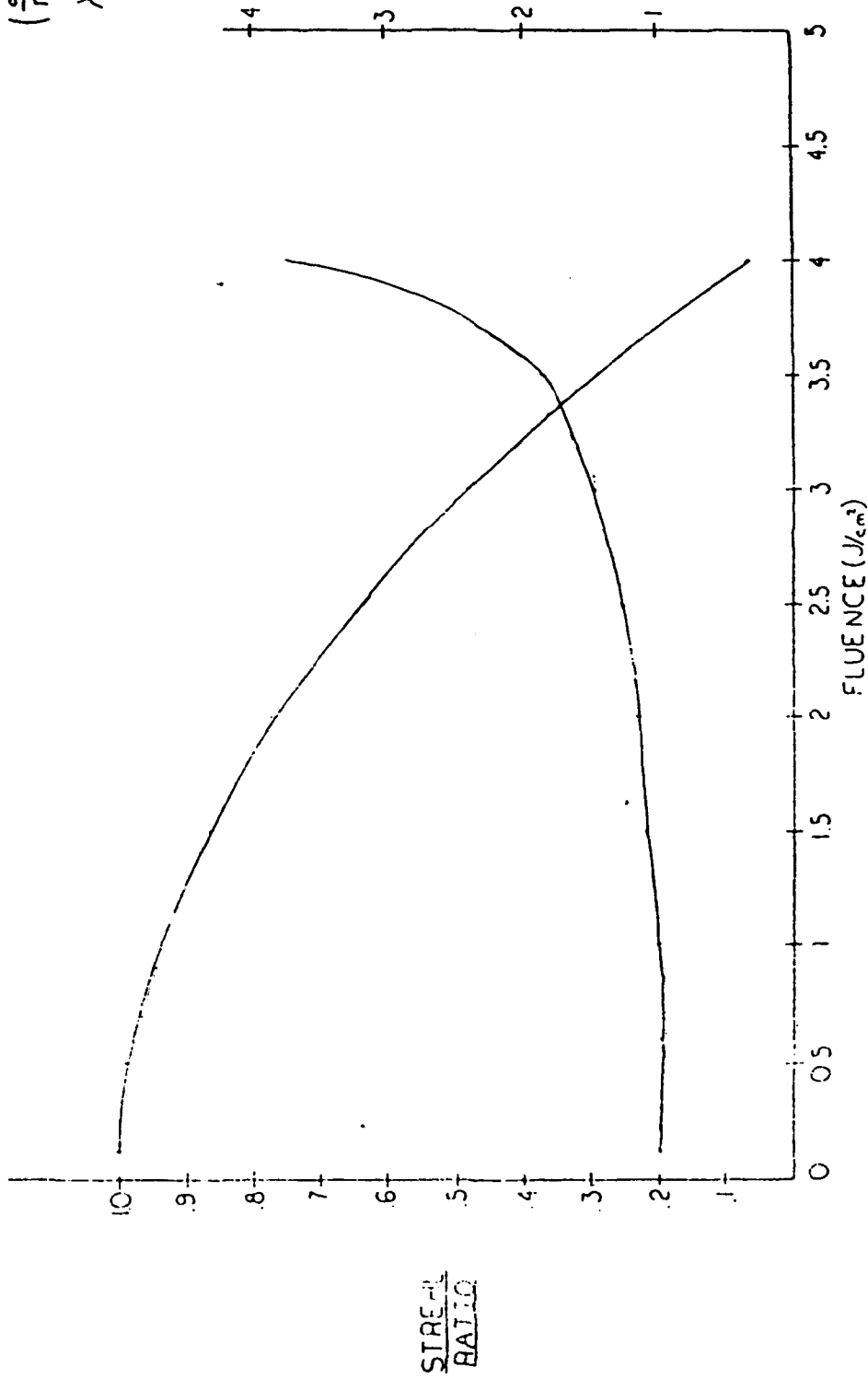



FIGURE 12

LASER TECHNOLOGY ASSOCIATES INC.			
No.	Revision	Date	By
Scale: N/A (Schematic/Computer Aided Design) M.K.			
Date: 10/18/88 (10/18/88) (10/18/88) (10/18/88)			
STRAIGHT THROUGH DYE LASER			
Material: NONE		Part Number: B-0008	

repetition rates involved allow the replacement of the dye volume at least once between shots. Thus, average power effects are minimal.

(3) Dye Laser System Architectures

There are a number of considerations to take into account when deciding upon the appropriate system architecture to choose for a given laser application. These considerations are now discussed and include assessing parasitics and ASE, beam quality, and system conversion efficiency.

It has been found that due to the combined effects of ASE and parasitic oscillations in dye lasers, more efficient systems result if an oscillator/amplifier system is employed where the amplifier is either single or double passed. This fact is the result of the difficulty of suppressing ASE and parasitics in an oscillator only configuration and that ASE and parasitics are effectively suppressed in a loaded amplifier. In a loaded amplifier, an incident oscillator beam is used to extract energy from the amplifier as pumping occurs, and parasitics and ASE do not reach threshold. This fact is used in commercial dye laser systems where oscillator/amplifier systems are used to increase system efficiency.

Another aspect of choosing the correct system architecture involves considering the losses inherent in oscillator only systems. In any oscillator, the round trip losses are important because multiple round trips occur. This is even true for dye laser oscillators where typically many tens of round trips are involved. In fact, while losses are minimized in most oscillator designs, with the dye laser, that is particularly difficult to achieve since it is necessary to introduce wavelength dispersive elements into the cavity in order to obtain a reasonably narrow bandwidth. The round trip loss, in such configurations involving the use of diffraction gratings or birefringent tuners, can be large, and typically ranges from 10-50% depending upon the specific technique used. Thus, in dye laser oscillators, the extraction efficiency is typically low unless broadband output is desired. In order to surmount this problem, it is necessary to consider dye laser oscillator/amplifier configurations (this is often referred to as a MOPA or master oscillator/power amplifier configuration). The efficiency of a MOPA system is always larger than that of an oscillator only, due to the fact that most of the pump energy is used in the amplifier stage that has at most two amplifying passes, while only a minimum amount of energy is used to drive the inefficient dye laser oscillator.

In order to maximize system beam quality, the MOPA configuration is also preferred. Again, in oscillator only dye lasers, all of the pump energy is deposited in the oscillator. Because multiple passes (typically many tens) of the aberrated medium occur, the beam quality from an oscillator only will be worse than that obtained with an oscillator/amplifier configuration. In addition, the oscillator only configuration does not lend itself to the use

of nonlinear optical phase conjugation (OPC) techniques, which can be used to correct aberrations which occur during the pump/laser output pulse. While some small phase aberrations result from the oscillator, the effect is minimized by minimizing the amount of green pump energy. Only enough is used to produce the approximately few mJ required to completely saturate the following double passed amplifier.

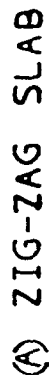
In order to overcome the thermal effects of degrading beam quality in dye lasers, two separate techniques may be considered, as shown in Figure 13. The first (a) involves the use of a zig-zag or slab dye laser amplifier. Such amplifiers have been demonstrated previously [17] and may be used to eliminate first order thermal focusing effects [18]. In order to practically implement this device, careful attention must be paid to achieving a good index match between the liquid and the materials used for the total-internal-reflection (TIR) faces, in order to minimize passive losses due to the many reflections. Another problem to be addressed is the flexing of the windows due to the dye cell internal pressure and changes in the operating pressure due to dye pump fluctuations. Birefringence effects do not occur in isotropic liquids, hence polarization losses due to bulk birefringence effects are absent in this configuration.

The second technique is to use the phenomena of Stimulated Brillouin Scattering (SBS) to double pass a dye laser amplifier. In this method the beam is focused after the first pass of the amplifier into an SBS cell that contains a liquid or a gas. SBS produces a backward traveling wave that is the phase-conjugate of the incident wave which removes the thermal aberrations of the amplifier media. The degree and fidelity of the compensation have been discussed recently [19]. It was shown unambiguously that the SBS reflectivity and fidelity depend only upon the focal spot intensity. As the magnitude of the aberration is increased, the reflectivity and fidelity both decreased monotonically as the focal spot size increased (intensity decreased). While these results were obtained at a wavelength of 355nm (tripled Nd:YAG) and using the medium hexane, similar results may be expected for methanol and ethanol, but with a somewhat larger reflectivity (75-85%). For the oscillator/amplifier dye laser considered here, sufficient energy/pulse is available after amplification by the first amplifier pass to achieve a focal spot intensity in an SBS medium many times above threshold. As shown previously in this Final Report, for incident green pump fluences of less than about 2.5 J/cm^2 which must be maintained to avoid optical damage to the dye laser dielectric coatings, a beam quality of less than three times diffraction-limited (see Figure 12) will be obtained after the first amplifier pass. This fairly mild range of aberrations will be corrected with good fidelity using the scheme shown in Figure 13(b). Note that since the beam brightness is inversely proportional to N , the number of times diffraction-limited, by eliminating most amplifier aberrations the beam brightness is improved by almost an order of magnitude.

167

M - MIRROR
P - POLARIZER

FIGURE 13



28

[illegible]

Scale: N/A References (or as Noted) Drawing: M K
Date: 3-22-89 10:01 AM Checked:

SYSTEMS TO IMPROVE
DYE LASER BEAM QUALITY

Material:	Part Number:	Drawing No.
	SAIR-8804	A-0071

LTA has devised a patentable phase-conjugated dye laser amplifier architecture that eliminates the need for a separate SBS cell by utilizing the geometry shown in Figure 14. The configuration is a MOPA, consisting of an oscillator followed by a double-passed amplifier, both pumped by doubled Nd:YAG. OPC is produced by using the dichroic mirror (DM) following the first amplifier pass to focus the beam into the flowing dye cell containing a dye/solvent mixture. The solvent is most often methanol, which has been shown to provide an excellent phase-conjugate reflectivity at 532nm [13]. The dye laser cell and SBS cell are one, therefore reducing the device space and volume requirements.

Due to the inherent simplicity of the dye laser MOPA system shown in Figure 14, we have chosen this approach over the dye slab laser approach shown in Figure 13(a). The dye slab laser requires precisely flat TIR surfaces, and complete insensitivity to ambient or fluctuating pressure within the dye cell. In addition, unless the dye solution and TIR plates are closely index matched the losses can become severe due to the multiple bounces. The phase-conjugated system shown in Figure 14 is clearly the simpler of the two approaches, will be less costly to manufacture, and will have less environmental sensitivity than the dye slab laser. It is our intent to demonstrate the system shown in Figure 14 in a Phase II contract.

IV. Tunable Dye Laser Modeling:

We have completed detailed modeling of the 532nm pumped organic dye MOPA system, including the second harmonic generation process (SHG). We begin by summarizing our SHG modeling results.

(a) Second Harmonic Generation:

The equations describing SHG are given by:

$$\begin{aligned}\frac{dE_1}{dz} &= \frac{1}{2k_1} \nabla_1^2 E_1 + \frac{ik_1}{2} \left[\left(\frac{n_1}{n_{10}} \right)^2 - 1 \right] E_1 - \frac{g_1 E_1}{2} - iK_1 E_1^* E_2 e^{-i\Delta kz} \\ \frac{dE_2}{dz} &= \frac{1}{2k_2} \nabla_2^2 E_2 + \frac{ik_2}{2} \left[\left(\frac{n_2}{n_{20}} \right)^2 - 1 \right] E_2 - \frac{g_2 E_2}{2} - \frac{iK_2}{2} E_1^2 e^{i\Delta kz}\end{aligned}\quad (16)$$

Here, E_1 and E_2 are the first and second harmonic fields respectively, $*$ denotes the complex conjugate, and K_i is defined as:

$$K_i = \frac{8\pi\omega_i^2 d_{eff}}{k_i c^2} \quad (17)$$

The quantity d_{eff} in Equation 17 is the second-order nonlinear coefficient. For KD*P, a commonly used SHG crystal available in large pieces with good optical quality, it has been found [20] that $K_1 = 1.4 \times 10^{-6} / V$, and $K_2 = 2K_1$. In Equation 16, the first term

LEGEND

SN37=7

P=POLARIZER

DM=DICHROIC MIRROR

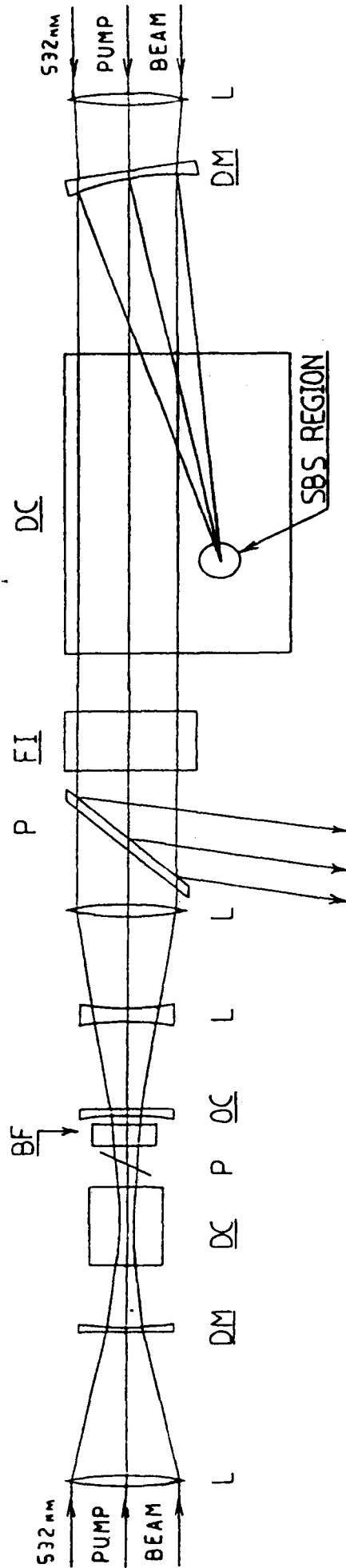
DC=DYE CELL

BF = BIREFRINGENT FILTER

FI = FARADAY ISOLATOR

OC = OUTPUT COUPLER

FIGURE 14

[illegible]

LASER TECHNOLOGY ASSOCIATES INC.

Scale:	N/A	References (or as noted)	Drawing: M.E.K.
Date:	7/6/80	Issued by: J.Y. XXX Issued to: J.P.O. 5	Checked:

Date:	8/9/11	Time:	10:01 AM
Checked:		By:	J. J. Jones

OPC DYE LASER SYSTEM

Material:	N/A
Part Number:	SATR-8804-K
Drawing No.	A-0009

on the right hand side represents beam diffraction, the second radial (or x-y) phase distortion that arises from crystal heating or nonlinear effects, the third, linear background absorption, and the fourth, the nonlinear coupling between the first and second harmonic waves. Δk is the phase mismatch between the second harmonic and fundamental waves, given by:

$$\Delta k = k_2 - 2k_1 \quad (18)$$

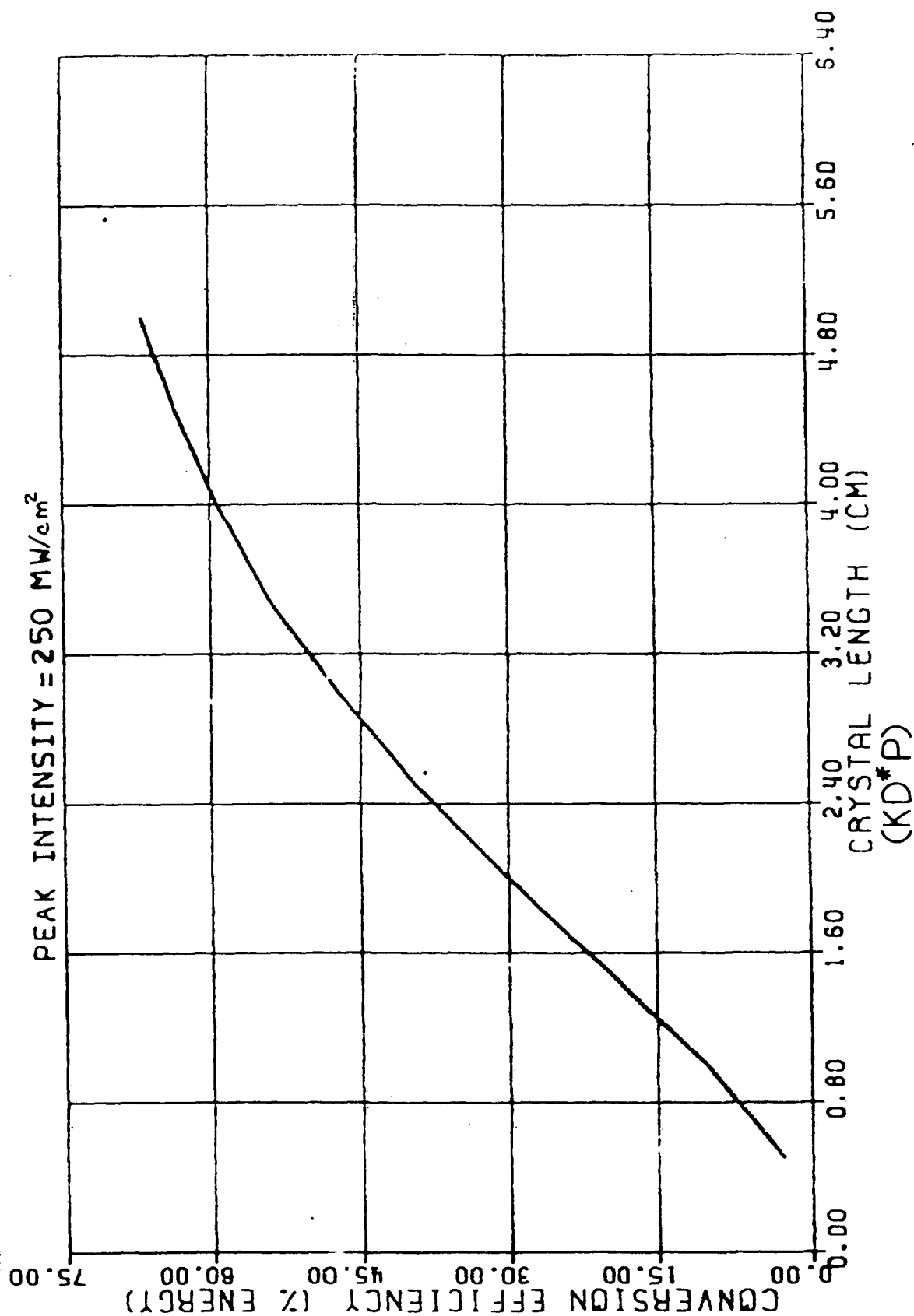
where k_1 and k_2 are the fundamental and second-harmonic wave-vectors, respectively. The LTA beam propagation code, discussed previously in this Final Report, is capable of diffractively propagating the fundamental and resulting second-harmonic beams through a nonlinear crystal, including the effects of diffraction, linear absorption, and phase distortion. The phase mismatch at any position on the wavefront is determined by calculating the normal to the wavefront in comparison to the optimum phase-matching direction. Our implementation of this propagation code is finite-difference in form. The wavefront is "marched" along the z-axis in a sequential way. For the purposes of this Phase I feasibility study we have assumed perfect phase-matching ($\Delta k=0$), and that crystal heating effects due to fundamental absorption are minimal. We have further assumed that the incident fundamental beam is Gaussian both temporally and spatially, and with a pulsewidth (FWHM) of 5ns, and a beam waist radially of 0.244 cm. The fundamental pulse energy was 250 mJ, and the beam waist chosen to be at the typical KD*P damage limit (peak intensity) of 250 MW/cm².

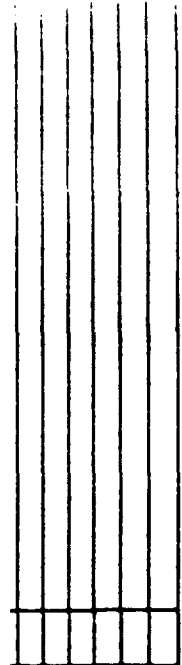
In Figure 15 we show the energy conversion efficiency from the (1064nm) fundamental to (532nm) green output energy, plotted as a function of crystal length, for the Type II doubling implementation shown in Figure 16. For maximum conversion the incident polarization vector is at 45° to the crystal e- and o-axes, resulting in an equal number of photons. Note that as the crystal length is increased, conversion efficiency does also, but not linearly. For a zero absorption coefficient at 1064nm and 532nm, near unity conversion would result if propagation was allowed to continue. Inclusion of typical background losses of 0.05/cm at 1064nm, and 0.005/cm at 532nm results in a less than unity asymptotic value. For the allowable damage intensity of 250 MW/cm², it is clear from Figure 15 that crystals of about 2.8 cm thickness are needed to reach a 50% conversion efficiency, and about 4.2 cm to reach 60% conversion. Crystals of this thickness are routinely available from a number of commercial sources.

If the assumed perfect phase-matching condition is broken, for example, by induced transverse temperature gradients leading to local index of refraction changes, it is clear that the types of conversion efficiencies shown in Figure 15 will be degraded. In fact, if phase-matching is broken, reconversion of some of the green light back into red light occurs, in agreement with earlier published work [21]. Minimizing crystal thermal gradients and phase aberrations on the fundamental beam are important to ensure that good conversion results. It should be mentioned that signif-

FIGURE 15

CONVERSION EFF. VS. CRYSTAL LENGTH



[illegible][illegible][illegible][illegible]

icantly larger conversion efficiencies would result if larger damage thresholds were allowed and if the crystal nonlinearity is larger. Both of these conditions are satisfied by using the relatively new nonlinear crystal BBO [2], which has a reported damage threshold of 13.5 GW/cm² for a 1 ns duration pulsewidth, and a nonlinear coefficient nearly ten times larger than that of KD*P. As larger crystals of this material become available (in cm sizes), conversion efficiencies in the range of 70-80% will become possible.

For the Gaussian fundamental beam described in connection with Figure 15, we have also obtained transverse profiles of the incident and exit 1064nm beam (shown in Figure 17 with both normalized to 1), and the exiting green profile shown in Figure 18. Both Figures are for a beam in KD*P after propagating through a 3.5 cm crystal. It can be seen by comparing these two Figures that a large part of the incident Gaussian, corresponding to the most intense portions, has been converted to 532nm light. This type of behavior is also seen temporally. As indicated by these results, the most efficient conversion is obtained for temporally and spatially flat-top pulses. While spatial flat-tops can be obtained in certain situations, the production of temporal flat-tops is not easily achieved.

For the purposes of this Phase I feasibility study, we assume from these results that a SHG efficiency in the range of 45-55% can be achieved in reasonably sized crystals, even in the presence of beam aberrations and somewhat non-perfect phase-matching. Undoubtedly, using a well-designed fundamental laser, with perhaps OPC or by using a crystal such as BBO, larger values can be achieved.

(b) Dye Laser Oscillator Modeling:

We have completed a rather detailed computer code that models the performance of laser oscillators. The code can be used to study and optimize the performance of any laser oscillator, and incorporates a number of important effects, including:

- (1) Oscillator buildup from spontaneous emission noise.
- (2) Diffraction.
- (3) Laser rate equations, including stimulated emission, passive losses, induced losses, energy transfer, etc.
- (4) Longitudinal laser pumping.
- (5) Standard or ring laser configurations.

The code is based upon the paraxial equation (3) discussed previously in this Final Report. Implementation is accomplished by a forward marching finite difference technique. Diffraction, phase distortion, and nonlinear effects are easily incorporated. The code propagates beams in the +z and -z direction simultane-

FIGURE 17

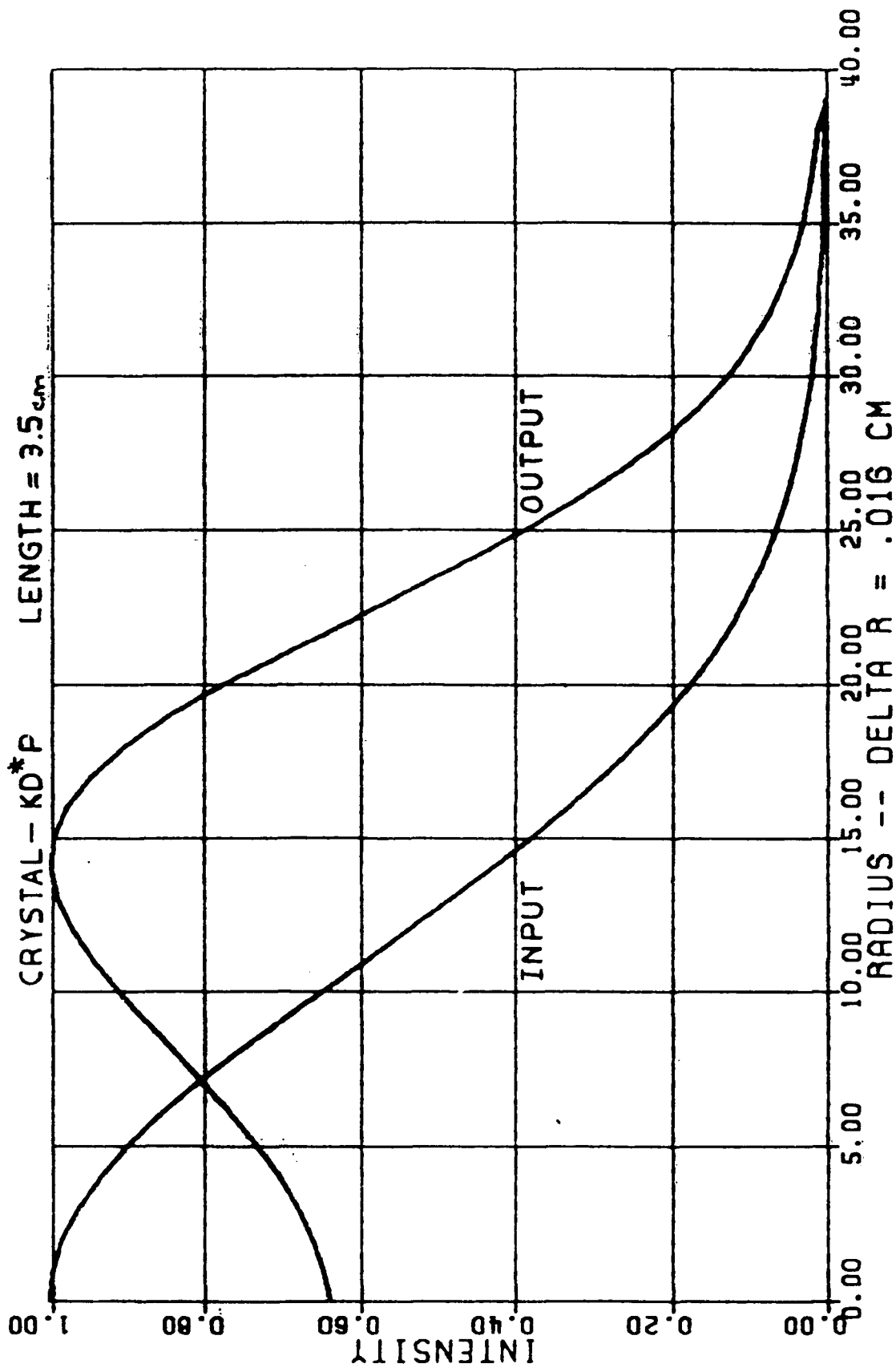
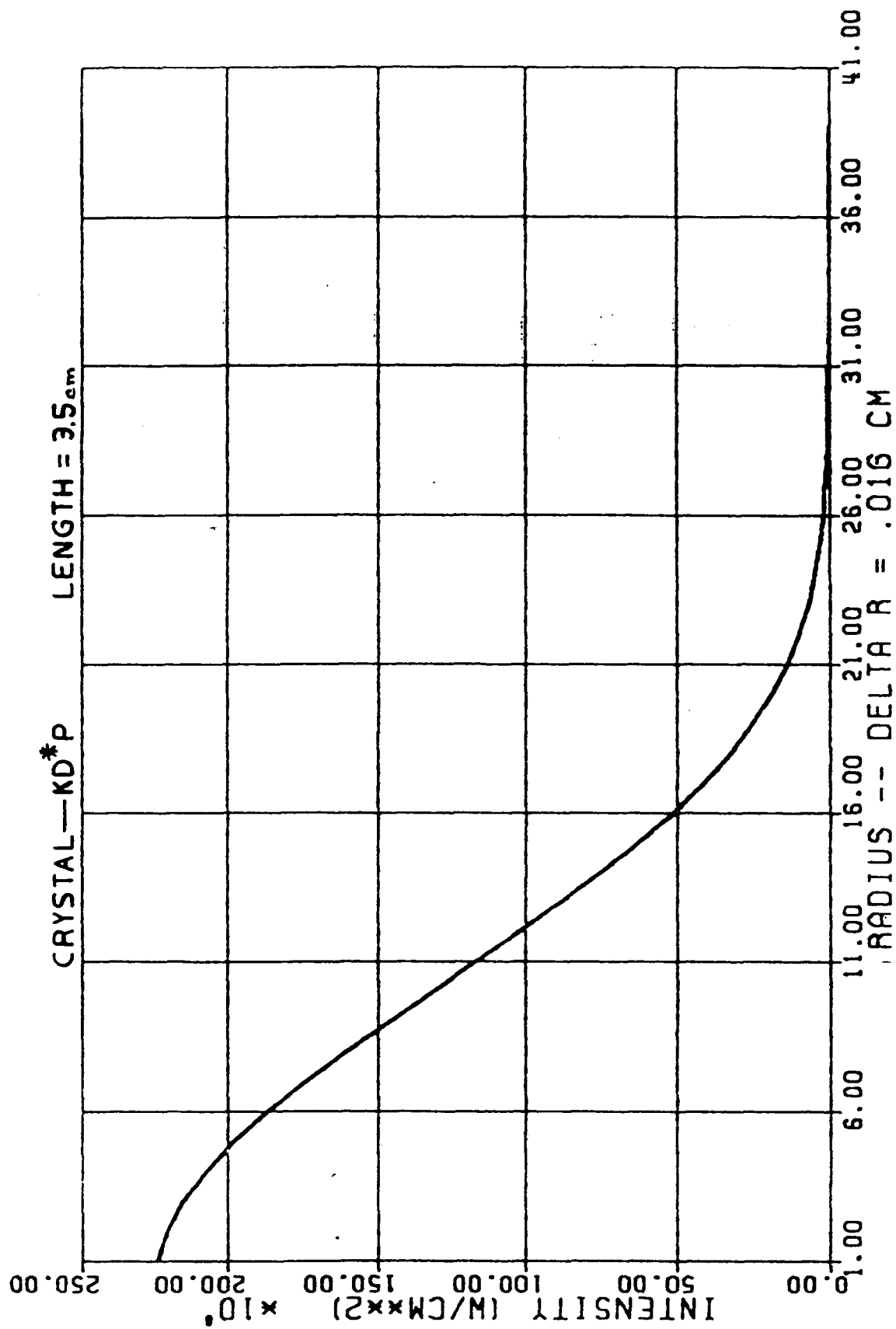
INPUT/OUTPUT BEAM PROFILES @ 1064_{nm}

FIGURE 18

532 nm OUTPUT PROFILE



ously. In order to model the dye laser oscillators of interest here, we have included the dye laser rate equations discussed previously (10 and 11). The pump beam, with wavelength 532nm, is diffractively propagated into the oscillator from either the +z or -z direction through a dichroic mirror forming one end of the oscillator cavity. The dichroic is assumed to be totally reflecting for the dye laser wavelengths of interest. The output coupler forms the other end of the cavity. As each of the two cavity circulating waves is incident upon the outcoupler the appropriate amount of intensity is allowed to leave the cavity. For the simulations described here, radial symmetry was assumed. Simulations were thus 2-D (r,t).

It should be mentioned that because of the typically large gains associated with dye lasers, ASE is a well known dye laser loss mechanism. While LTA has broad experience simulating ASE effects in various laser devices, at present we are limited by computer speed and cannot include the effect in our analysis. Nevertheless, the results we present here are, as we will see below, correct at least qualitatively. In fact, all the known features of laser pumped dye lasers have been reproduced here. Neglecting ASE in our dye laser oscillator analysis is not important at present because only a fraction of the green pump is used to pump the oscillator. Most of the green energy is supplied to the dye amplifier where the effects of ASE are more well controlled. The amount of error caused by ignoring ASE cannot really be assessed without an experimental data base which is not available at present. This data base will be generated during a Phase II program.

For the purposes of this Phase I program, we have chosen to concentrate only on the dye Rhodamine 6G. Spectral properties of this dye have been shown previously in Figure 11. This dye lases in the spectral region of interest here and is by far the most well characterized dye at present. This is not restrictive since other dyes can be easily simulated as well using this code. The dye concentration used in these simulations was chosen so that 99% of the green pump energy is absorbed after a single pass. Our dye cell was assumed to be 4 cm in length and had a concentration of 6×10^{-6} M. 20 mJ of green pump energy was used to drive the oscillator. The pump pulse had a FWHM of 5ns, typical of frequency doubled Nd:YAG lasers. The total cavity length was 7 cm. A birefringent tuner was assumed to be used for wavelength tunability, with a transmission of 80%.

In Figures 19-22, we show the obtained oscillator output and the associated green pump pulse for output coupler reflectivities of 0.4, 0.5, 0.6, and 0.7, respectively. The wavelength was taken at the peak of the Rhodamine 6G stimulated emission cross-section curve (570nm). A number of features of these curves should be noted. The peak of the oscillator output curve is shifted from that of the green pump pulse, typically by about 2ns. The reason for this is of course the finite cavity buildup time. Note that because of this effect the green pump pulse used to drive the following amplifier stage should also be delayed by a similar amount. Another feature of the dye output pulse is the rapidly

OSCILLATOR POWER NORMALIZED

20 MJ PUMP

2.33 MJ OUTPUT

7 CM CAVITY

4 CM GAIN

$R = .4$

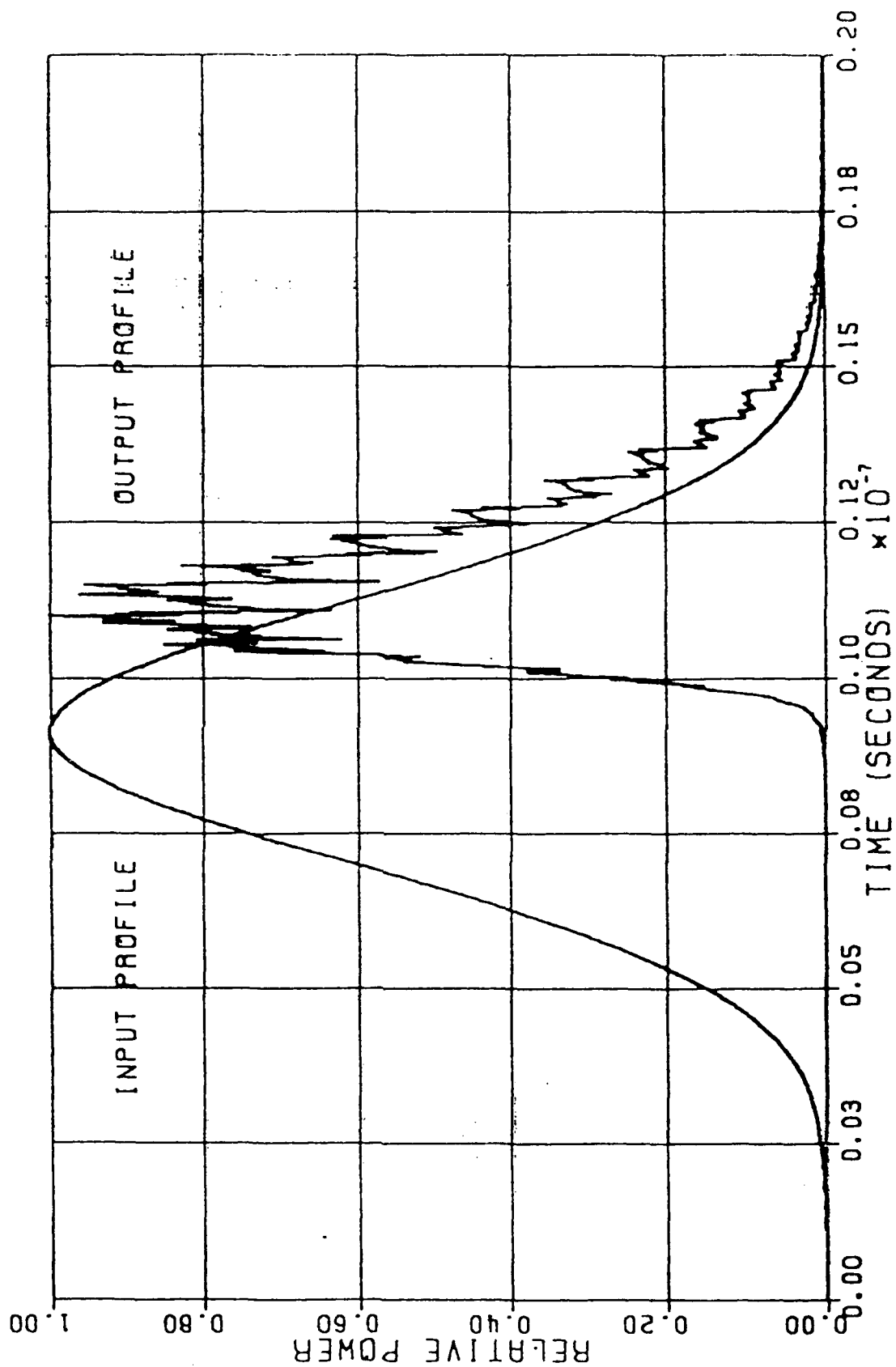


FIGURE 19

USCILLATION POWER NORMALIZED

20 MJ PUMP

7 CM CAVITY

4 CM GAIN

2.50 MJ OUTPUT

R = .5

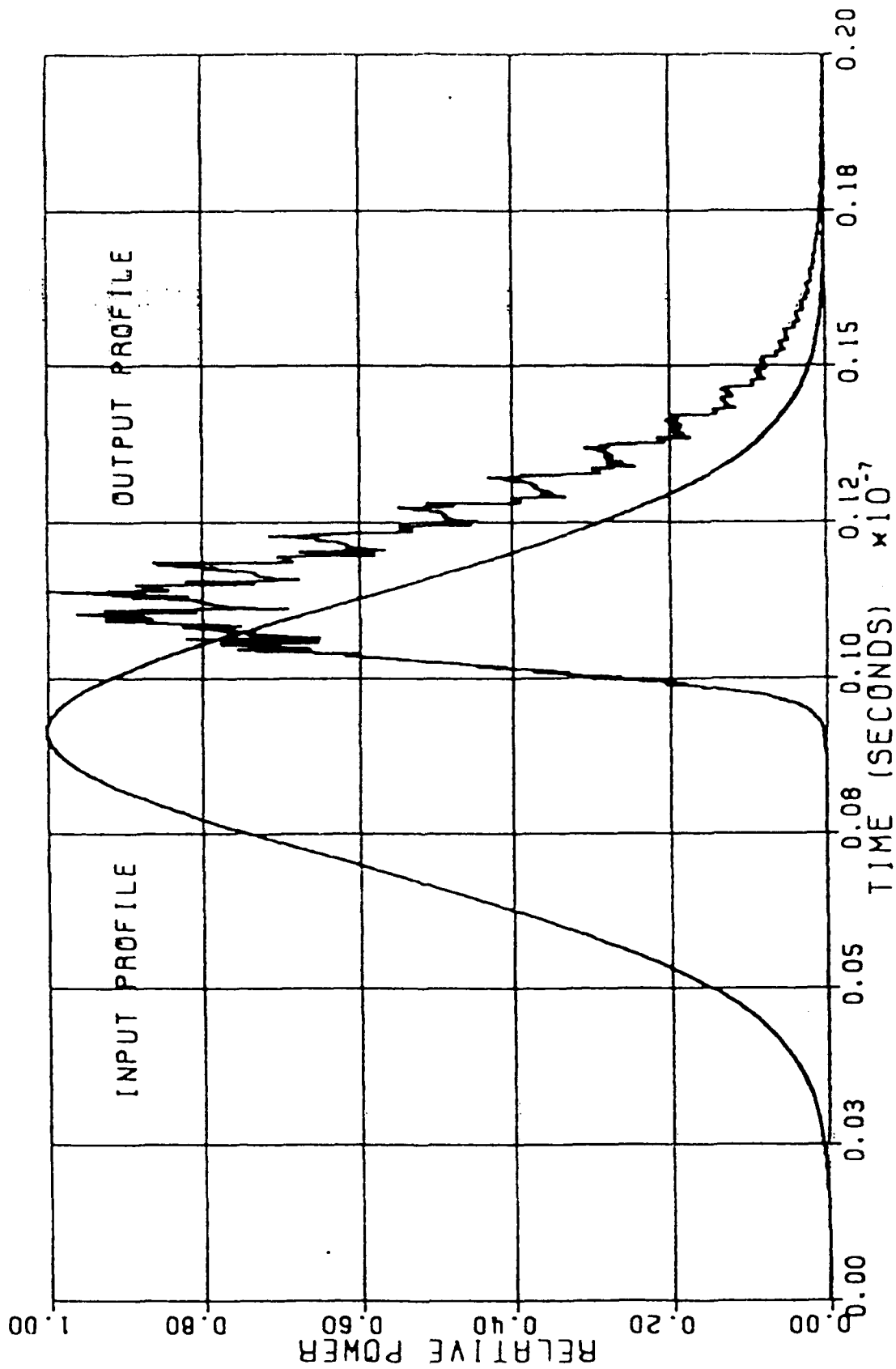


FIGURE 20

OSCILLATOR POWER NORMALIZED

20 MJ PUMP
2.50 MJ OUTPUT

7 CM CAVITY

4 CM GAIN

$R = .6$

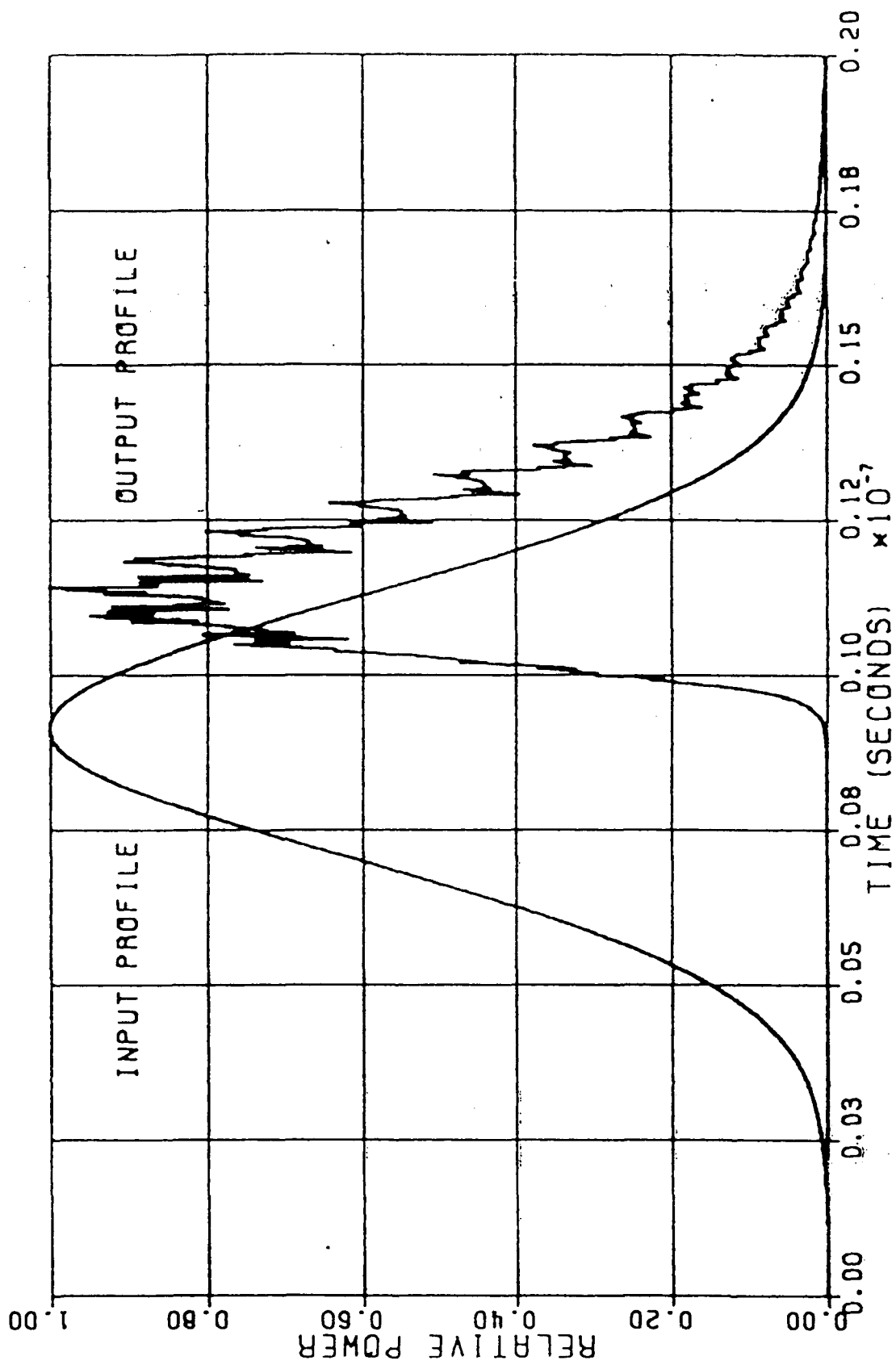


FIGURE 21

NORMALIZED

20 MJ PUMP
2.14 MJ OUTPUT

7 CM CAVITY

4 CM GAIN

R = .7

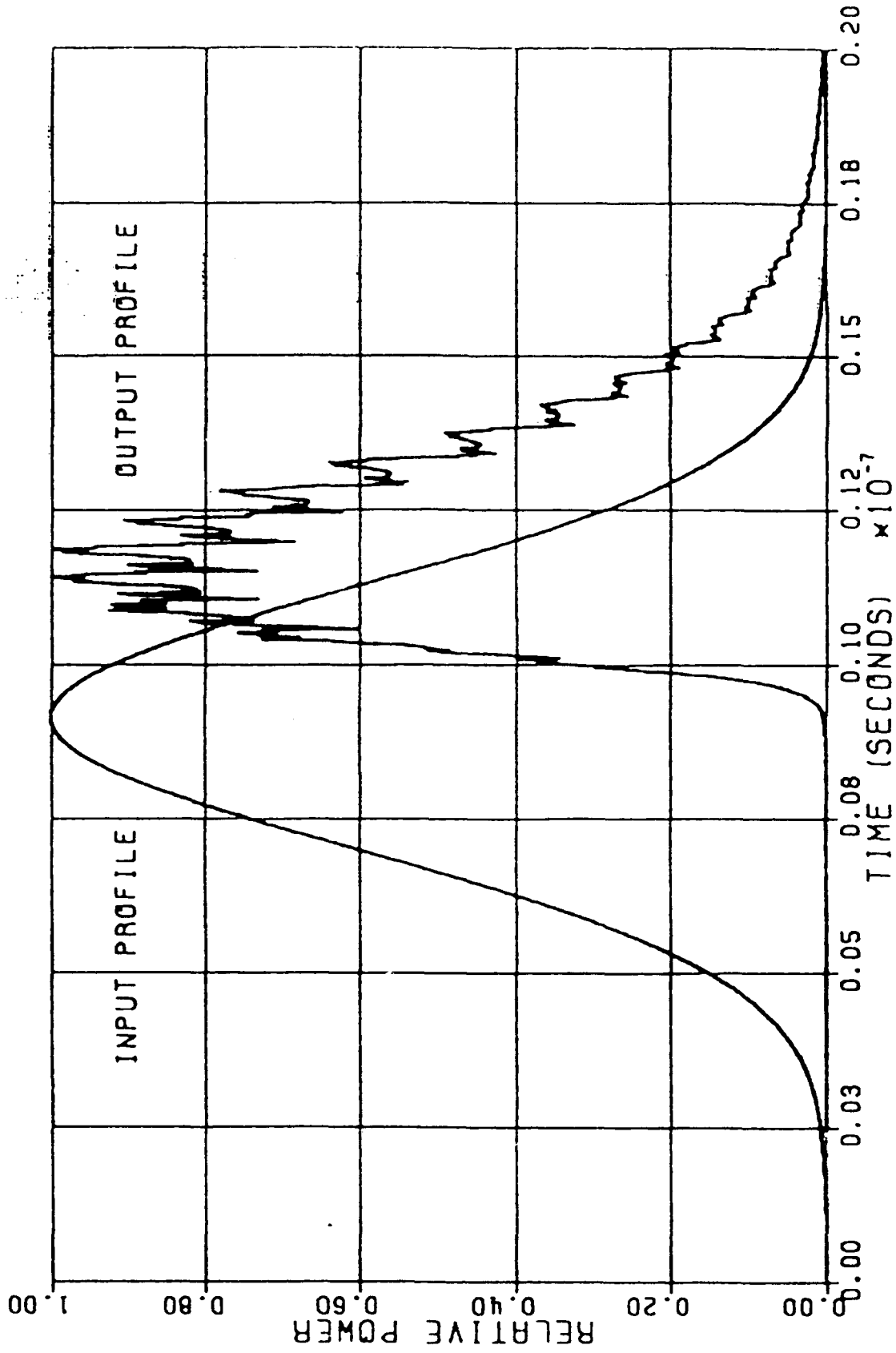


FIGURE 22

rising leading edge followed by a trailing edge. This and the time delay discussed above have both been seen experimentally. The sharp leading edge arises from the large amount of gain existing in the oscillator at threshold. Careful study of Figures 19-22 shows that the noisy nature of the dye laser output reveals a periodic structure. In fact the output consists of two sets of shorter picosecond duration pulses, one with a large and the other a smaller amplitude. Both sets of pulses are separated by the oscillator round trip time (0.47ns) and arise from the two circulating waves inside the cavity. Our simulations have shown that the amplitudes of both sets become equal if equal out-coupling is allowed at each end and vanish altogether if a ring laser configuration is used. These oscillations have been observed experimentally and predicted theoretically [22].

In Figure 23 the extraction efficiency is shown as a function of the outcoupler reflectivity. It can be seen that slightly over 12% of the green pump is converted to 570nm output, and that the optimum outcoupler is in the range of 50-60%. This corresponds to an energy/pulse of 2.5 mJ. Theoretically, from a quantum defect point of view, about 93% of the green pump energy can be converted to 570nm output. The reason for the rather low extraction efficiency is the insertion loss of the birefringent tuner.

Using our oscillator code, a number of other interesting and important effects can be predicted. Figure 24 shows the time evolution of the Rhodamine 6G upper level inversion density as a function of time. One observes that the upper level inversion increases to a rather large value before the oscillator circulating intensity builds up and significant extraction occurs. The sharp drop in inversion density corresponds to the steep leading edge of the oscillator output pulse (Figure 21). Some repumping of the dye is evident in Figure 24. In Figures 25-28, which correspond to Figures 19-22, respectively, we have plotted the on-axis round trip gain as a function of time. It is important to note that the analytical round trip small-signal gain is of the order of 10^4 for this case. Due to the depletion of the gain by the circulating waves, however, the actual saturated gain never approaches this value, but is maintained in the range of 30-36. Note that as the outcoupler reflectivity decreases the peak saturated gain increases since the circulating intensity is reduced.

In Figure 29, the oscillator output energy/pulse is displayed as a function of wavelength. The appropriate cross-sections and singlet absorption losses for Rhodamine 6G have been used at each wavelength. The precipitous drop in energy/pulse at shorter wavelengths is caused by a rapidly rising singlet absorption loss as wavelength decreases. The peak oscillator emission is located at 590nm, shifted from the location of the peak wavelength at 570nm due to the singlet absorption loss. At longer wavelengths, singlet absorption is minimal but the stimulated emission cross-section monotonically decreases. The values for the energy/pulse shown in Figure 29 were used as input to the amplifier simulations described in the next Section of this Final Report.

EXTRACTION EFFICIENCY

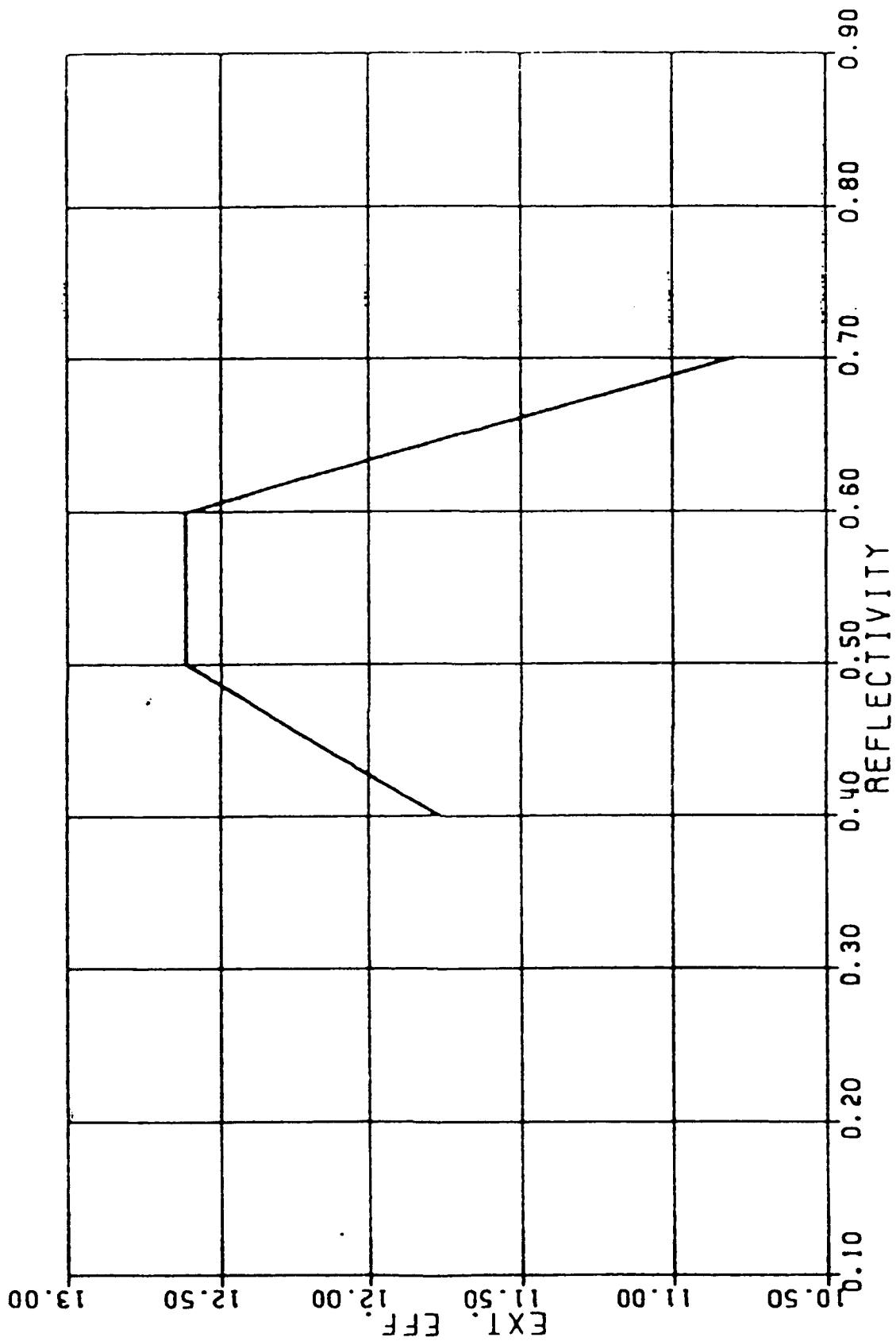


FIGURE 23

OSCILLATOR
UPPER LEVEL INVERSION

20 MJ PUMP

7 CH CAVITY

$R = .6$

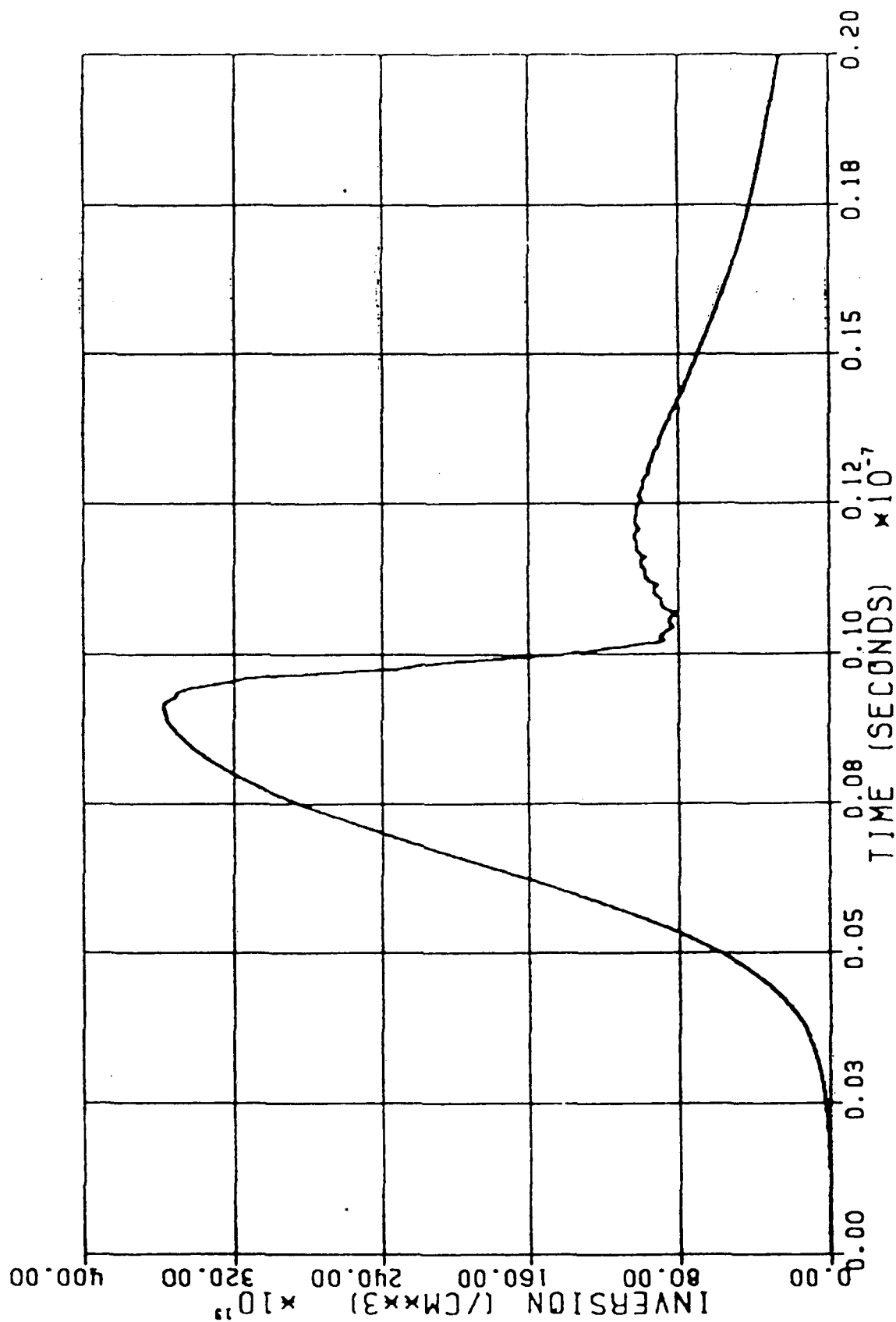


FIGURE 24

20 MJ PUMP
ULTRAVIOLET
ROUND TRIP GAIN
7 CM CAVITY
 $R = .4$

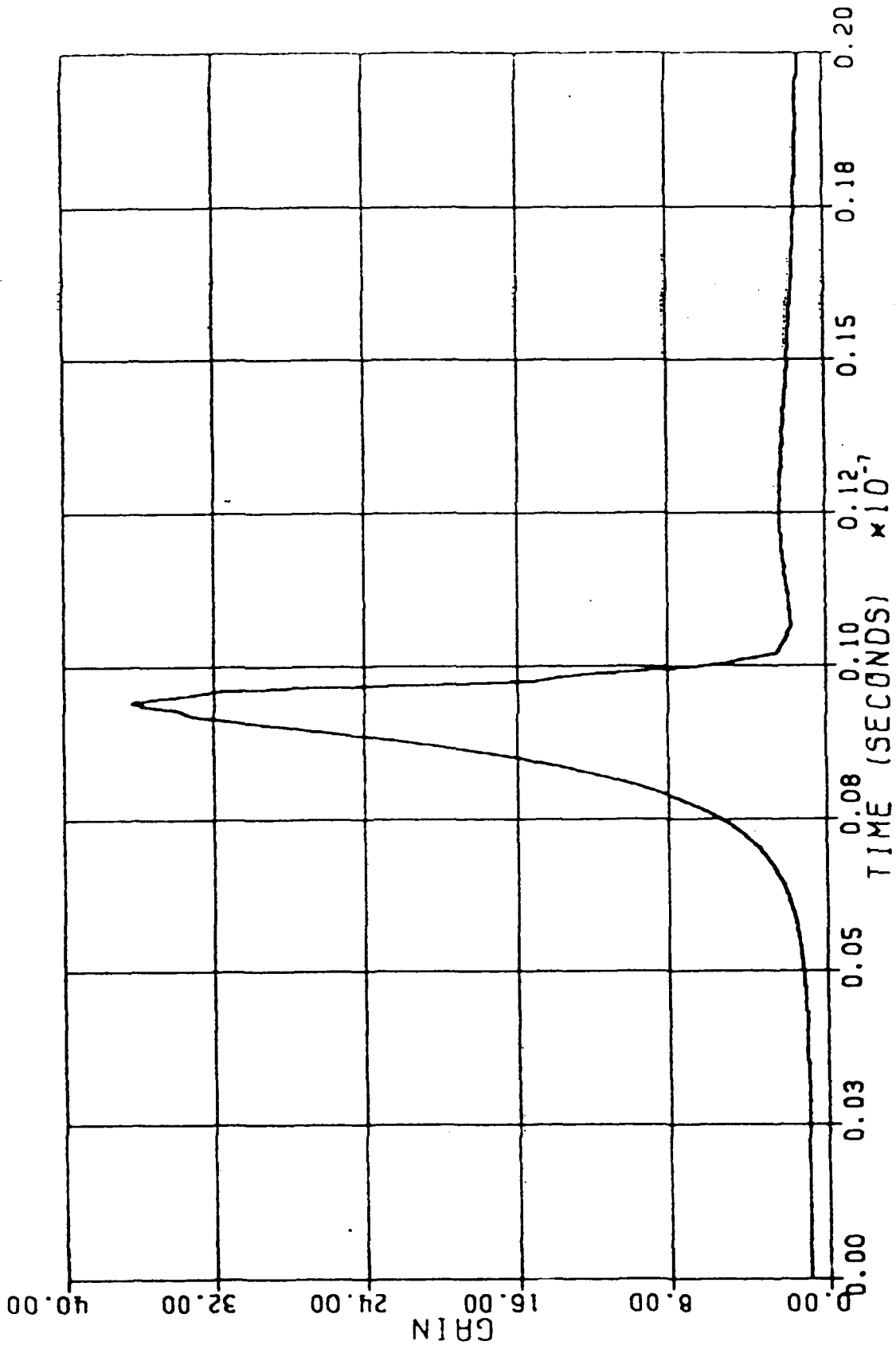


FIGURE 25

OSCILLATOR
ROUND TRIP GAIN

20 MJ PUMP

7 CM CAVITY

$R = .5$

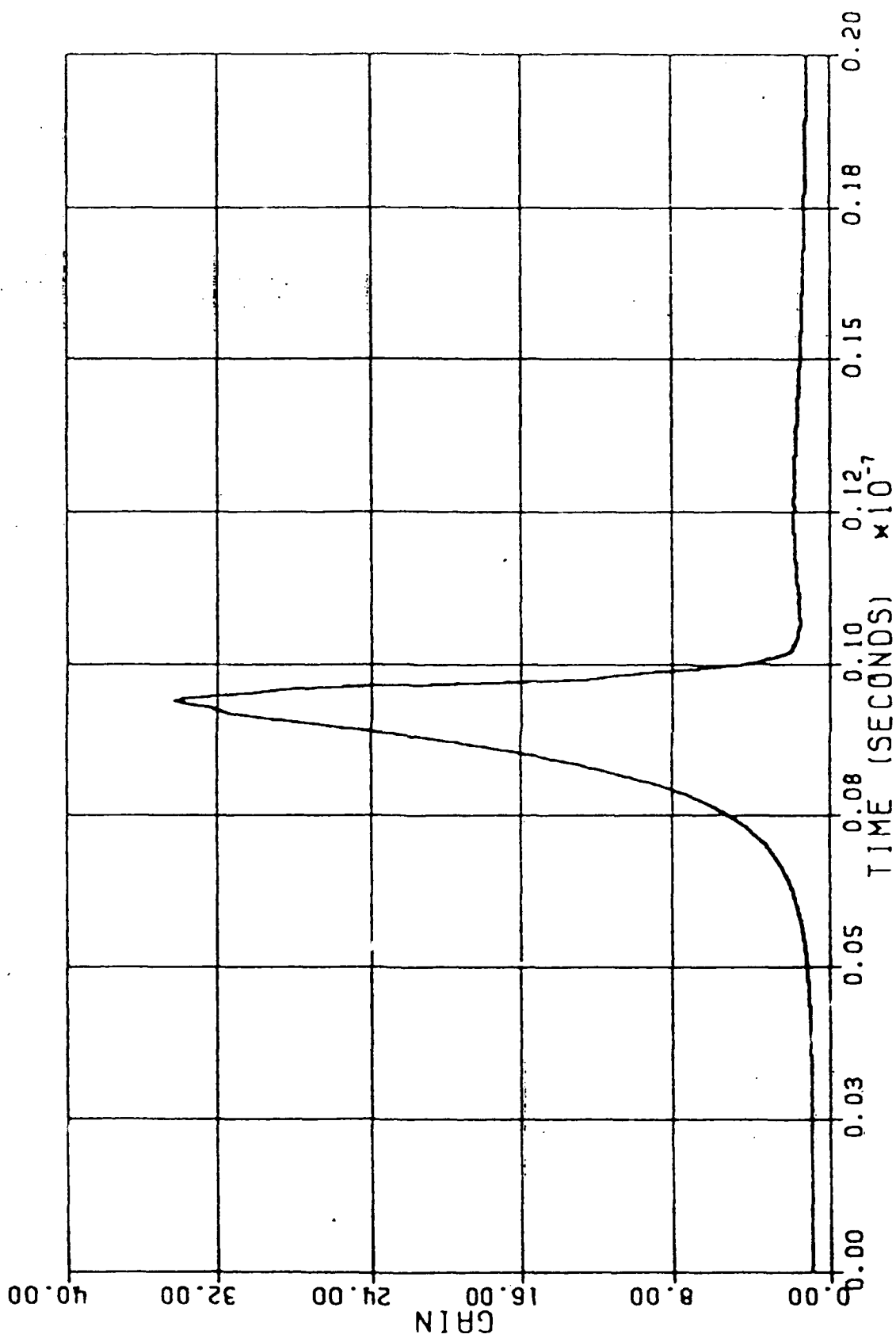


FIGURE 26

OSCILLATOR
ROUND TRIP GAIN

20 MJ PUMP 7 CM CAVITY $R = .6$

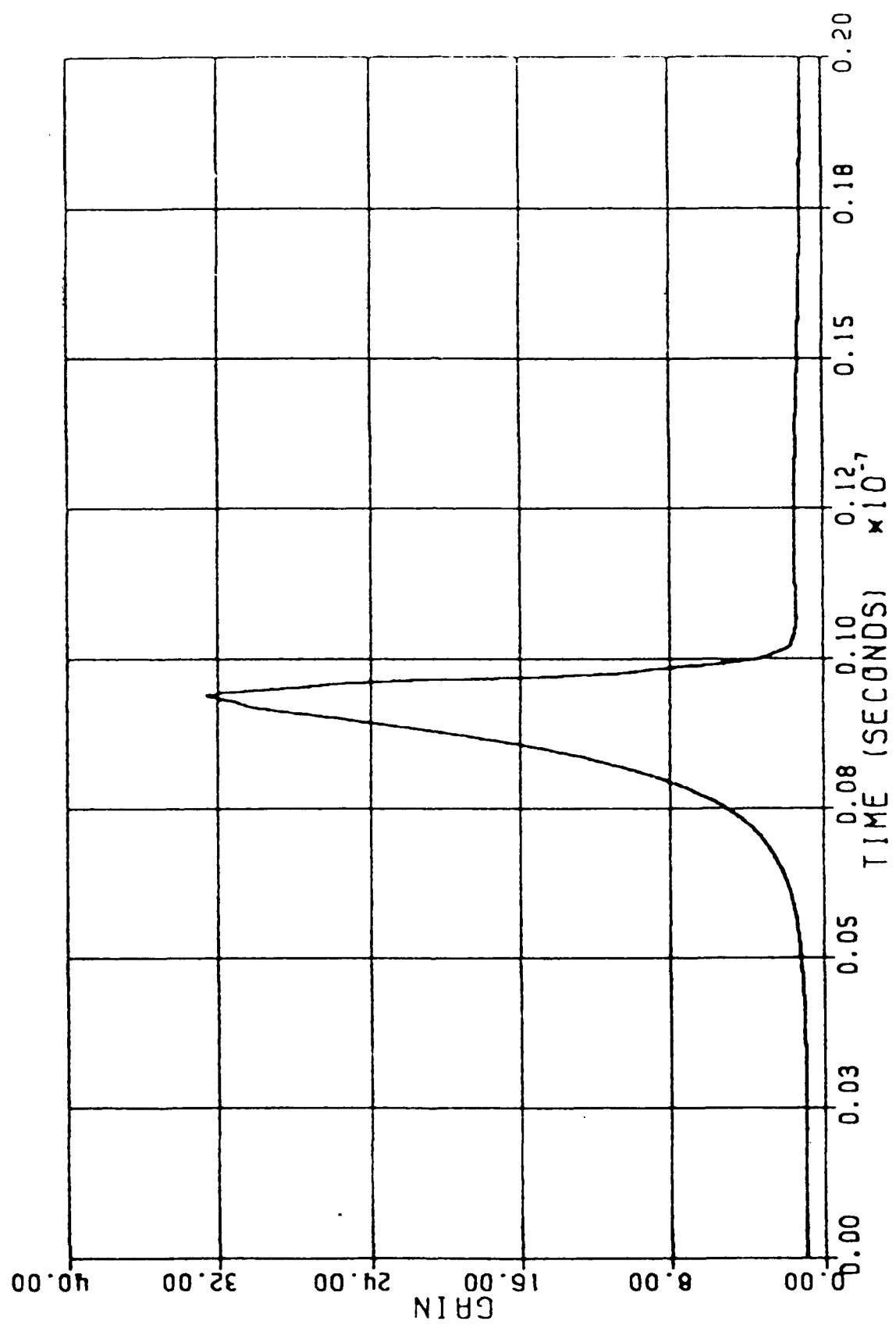


FIGURE 27

OSCILLATOR ROUND TRIP GAIN

20 MJ PUMP 7 CM CAVITY $R = .7$

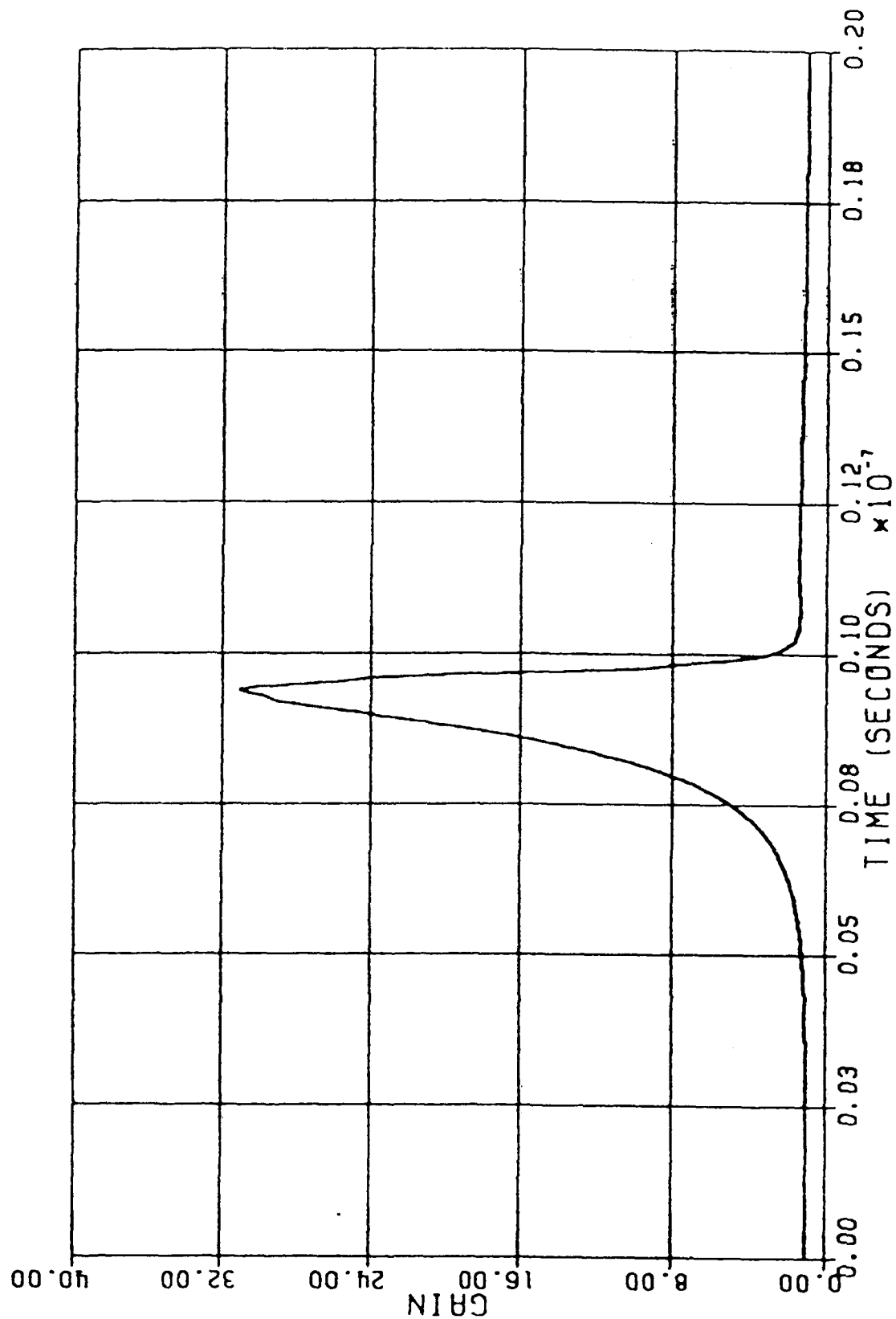


FIGURE 28

OSCILLATOR OUTPUT ENERGY AS
A FUNCTION OF WAVELENGTH

20 MJ PUMP

7 CM CAVITY

$R = .6$

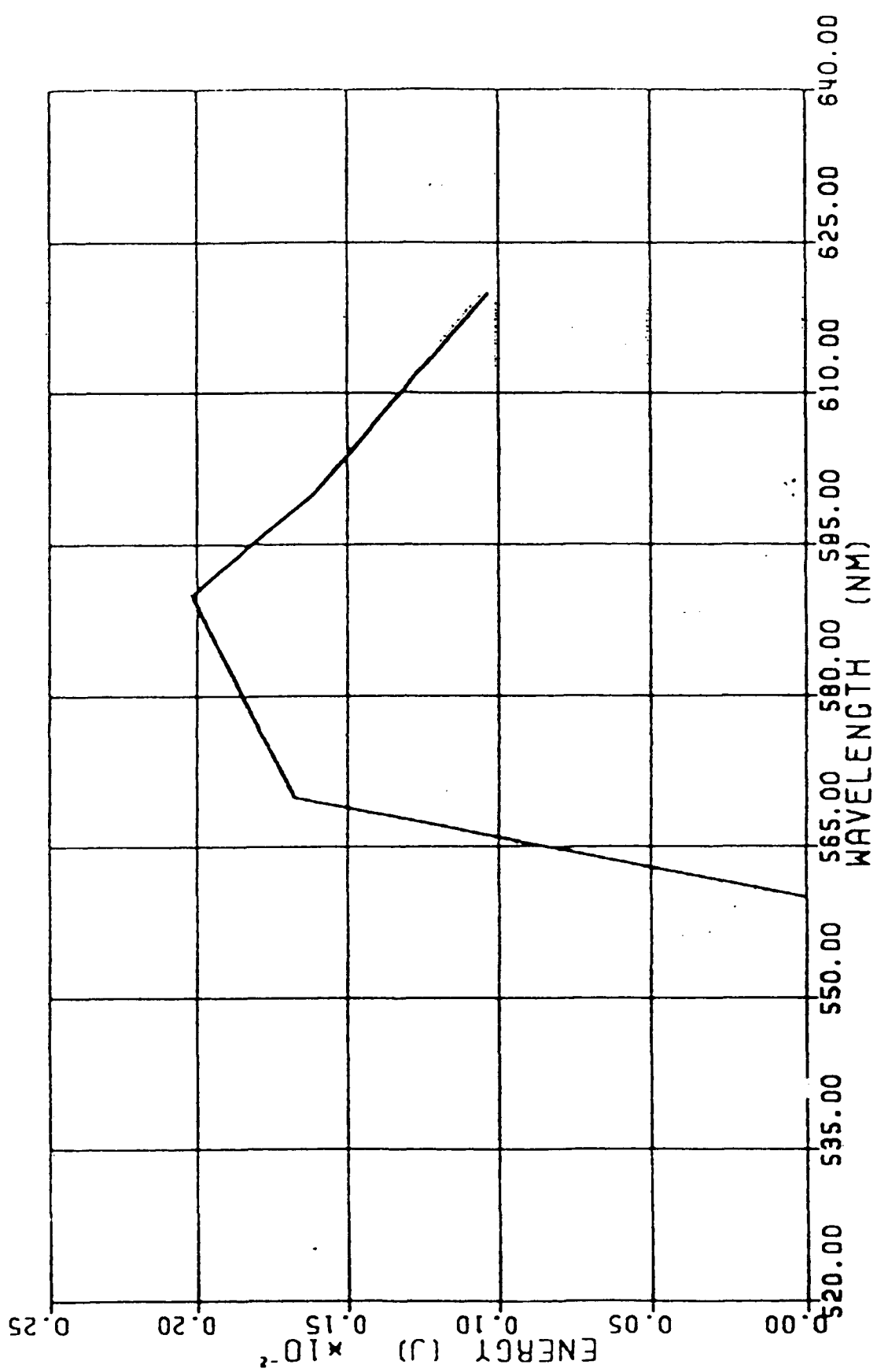


FIGURE 29

During this Phase I study, the question has arisen as to exactly how large the small-signal gain can be allowed to become before the effects of ASE and/or parasitic oscillations begin to dominate. In most lasers, it is prudent to allow a round trip gain of about 100. Increases beyond this value usually lead to significant energy loss due to parasitics that lase off secondary window or optics reflections or diffuse parasitics that can arise from surface scattering, even off optics or mounts that are external to the oscillator. It is clear that to increase extraction efficiency one would like to minimize the beam radius and thus maximize the extracting intensity. There is still room to further decrease our beam radius used in these simulations from the present range of 5-7 mm to only a few mm. Optical damage is not a consideration here since for 5 ns duration pulses, over 2.5 J/cm^2 of green fluence can be tolerated, corresponding to a beam radius of $1/2 \text{ mm}$. The maximum round trip gain that can be tolerated without unacceptable losses from ASE or parasitics will ultimately be determined by experiment in a Phase II SBIR program.

It is clear from the aforementioned oscillator results that all of the observed essential features of dye laser oscillators have been reproduced. In order for our code to be considered reliable in optimizing oscillators, it must be normalized to actual experimental results in the Phase II program. Other LTA codes, such as our pump cavity optimization code, has undergone extensive normalization with experiments, with very close agreement obtained.

(c) Dye Laser Amplifier Modeling:

In order to assess the potential overall efficiency of the dye laser approach we have also performed modeling of the double passed dye laser amplifier shown in Figure 14. In Figure 30, we show the extraction efficiency as a function of the extracting beam radius for a single and a double passed dye amplifier pumped with the remaining green energy (105 mJ/pulse), at a wavelength of 570nm and an input energy/pulse of 1.5 mJ. We have assumed here that the reflector or phase-conjugate mirror has unity reflectivity. It can be seen that the extraction efficiency is very good for either case, due to the large Rhodamine gain/cm, and improves as the radius is decreased. In the double passed case, the extraction for reasonably sized beams ($<0.5 \text{ cm}$) is greater than about 90%. Recall that the maximum extraction efficiency at the operating wavelength is 93%. While ASE and beam timing (the timing of the extracting pulse in relation to the pump pulse) will undoubtedly slightly decrease the actual extraction efficiency, it is evident that the double passed amplifier should provide an excellent extraction and overall efficiency, significantly higher than that obtainable with an oscillator alone.

In Figure 31 we show the obtained extraction efficiency as a function of wavelength for a fixed beam radius of 0.5 cm, and for reflectivities of 1.0, 0.9, 0.8, and 0.7. The green pump pulse is

FIGURE 30

EXTRACTION EFFICIENCY VS RADIUS SINGLE AND DOUBLE PASS

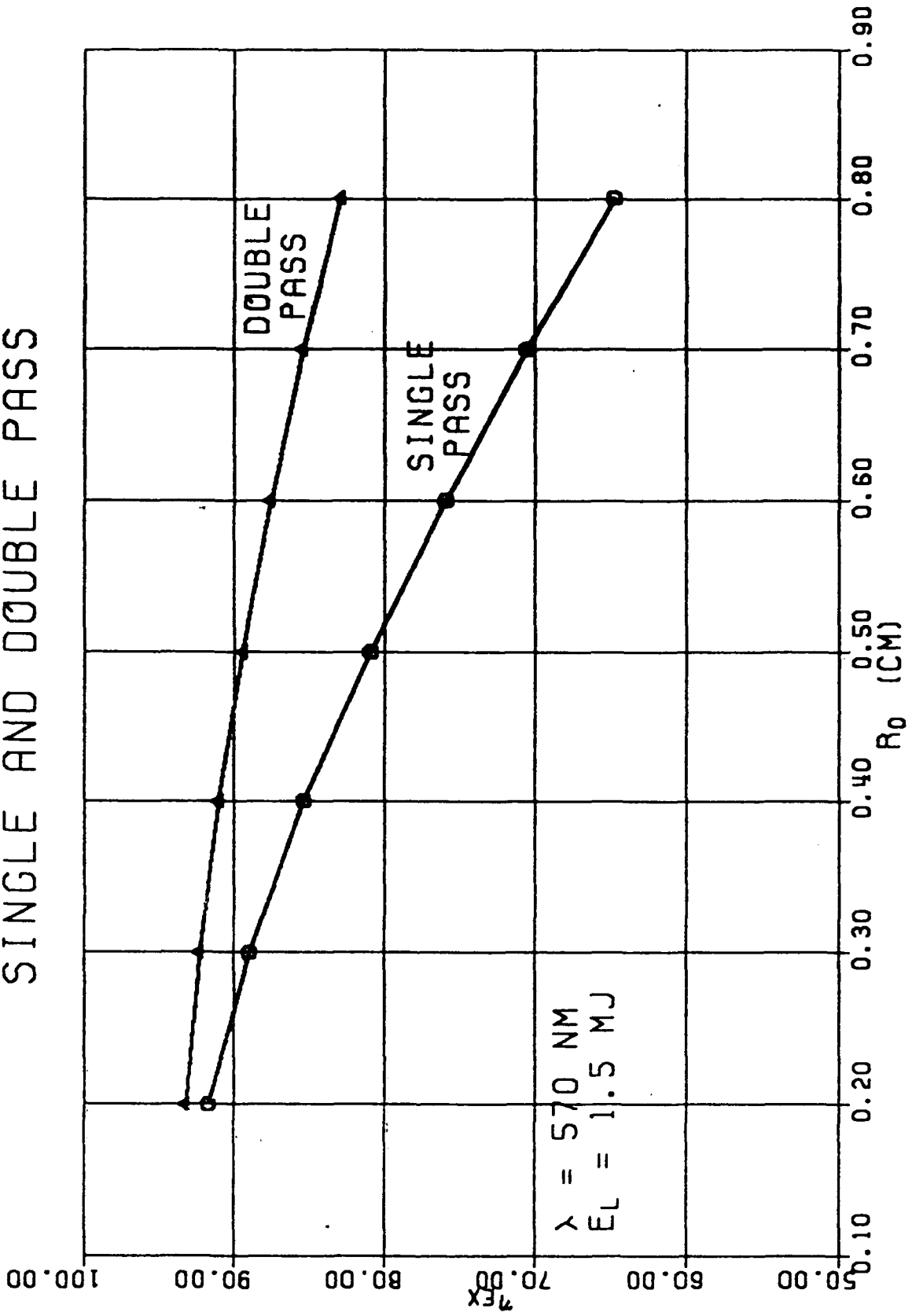
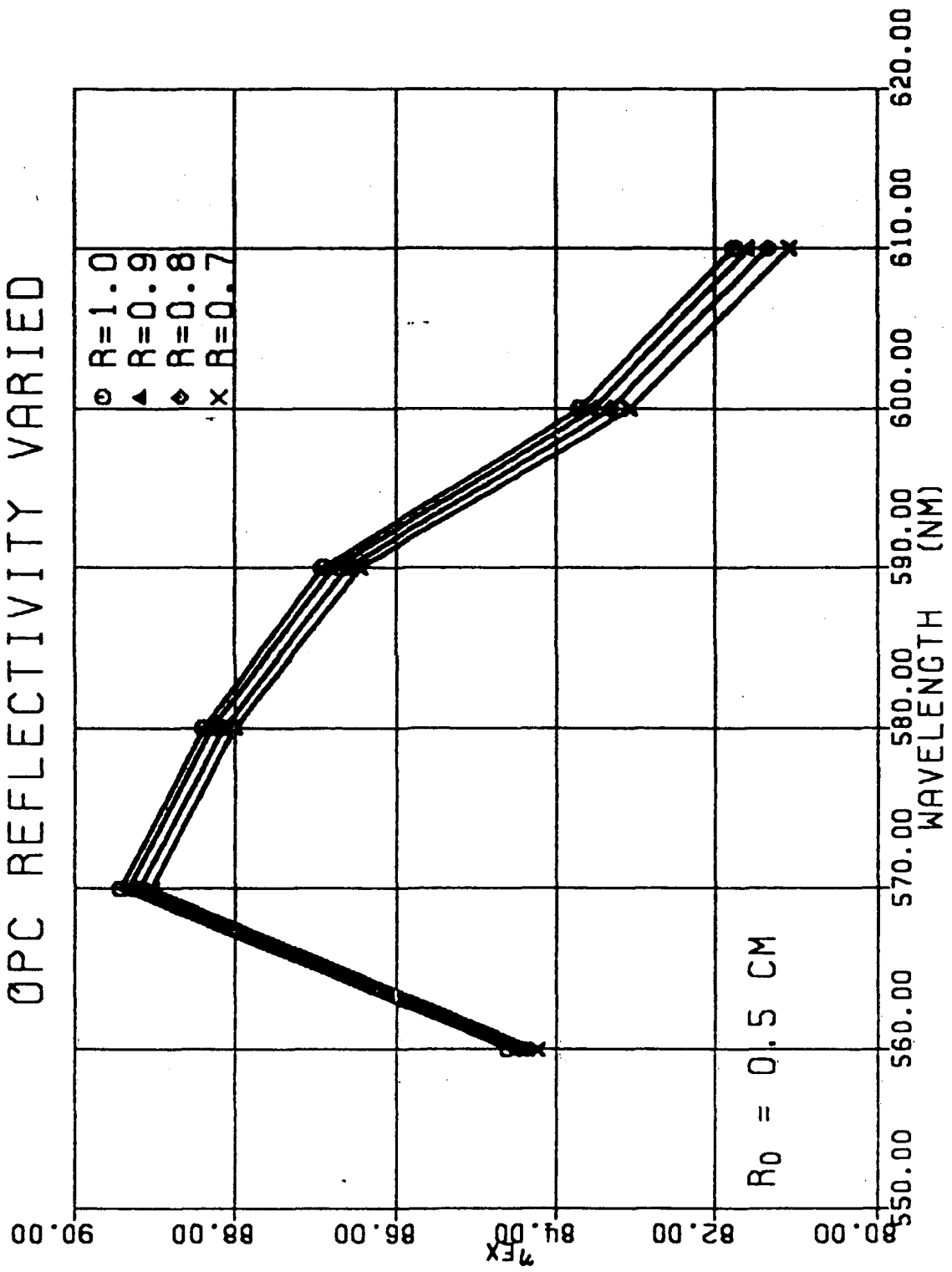


FIGURE 31
EXTRACTION EFFICIENCY VS WAVELENGTH
OPC REFLECTIVITY VARIED



again fixed at 105 mJ and the input varied according to Figure 29. It is significant that as the reflectivity decreases, the extraction efficiency varies only slightly, again a consequence of the high dye gain and highly saturated state of the amplifier. Two important conclusions can be drawn from Figure 31. First, as the wavelength and output of the oscillator vary, the extraction efficiency at any wavelength is still very good, exceeding 80% in all cases considered. Since with OPC the reflecting focusing mirror can be metallic with very little variation of reflectivity with wavelength, and SBS is essentially wavelength independent, this situation should be obtainable in the laboratory. The second conclusion is that with typical phase-conjugate reflectivity in the range of 75-85%, very little change in performance is expected if OPC is utilized to improve beam quality.

V. Conclusions:

In this Phase I SBIR program, we have assessed the current state-of-the-art in tunable visible laser technology. As discussed earlier in this Final Report, we have chosen the tunable dye laser approach from amongst the various candidate systems as the one with the most near term potential for improvement. Our baseline approach, shown previously in Figure 14, involves utilizing an oscillator/double-passed amplifier system. Double passing of the amplifier is accomplished by use of SBS in the dye cell. Dynamic amplifier distortions are eliminated using this technique. A further advantage of this approach is that the conversion efficiency from 1064nm Nd:YAG output to dye laser output (overall conversion efficiency) can be quite high, and as shown in the previous section, nearly wavelength independent. For the purposes of the initial systems comparison discussed earlier in connection with Table 1, we assumed a SHG efficiency in the range of 45-55%, and a dye laser extraction efficiency in the range of 3-55% for a green (532nm) pump. After the more detailed modeling of the dye laser approach and SHG described in the aforementioned, we now estimate the following efficiencies.

For SHG we assume, based upon our modeling, that a practical SHG efficiency is in the range of 45-55% for KD*P under thermally loaded conditions. For the newer crystal BBO, practical efficiencies of 70-80% can be obtained due to the larger damage threshold and higher nonlinear coefficient. For the dye laser, using Figure 31 and the previous results on the dye laser oscillator, we estimate that the overall dye laser extraction efficiency will exceed 70% for any wavelength, using a double-passed phase-conjugated configuration. The overall conversion efficiency from 1064nm output to dye laser output is then in the range of 32-39% if KD*P is used, and in the range 49-56% for BBO. The previous best estimate of 14-30% shown in Table 1 for dye lasers is thus conservative.

The results obtained here should be contrasted with typical green pumped dye laser oscillators that typically achieve a dye laser extraction efficiency of 50%, and a SHG efficiency of 40-50%, or an overall efficiency of 20-25%. Using the configuration shown in

Figure 14, a substantial improvement in the beam quality and overall conversion efficiency of visible dye laser systems can be obtained.

VI. Summary of Recommended Phase II Program:

LTA intends to submit a proposal for a Phase II SBIR program shortly, based upon the innovative approach to a dye laser MOPA system and the modeling we have completed during the Phase I feasibility study. We have shown the substantial improvements that can be obtained by utilizing a dye laser MOPA approach and OPC. Substantial increases in beam quality (brightness) and overall conversion efficiency can be obtained using our approach. The unique OPC design that utilizes the dye cell as the phase conjugation medium can lead to an efficient tunable visible laser source that is also compact.

During our proposed Phase II program, we will construct the dye laser shown in Figure 14 and determine its salient operating characteristics. An important part of the Phase II experimental program will be to determine exactly how important ASE effects are in a practical device, and to include the ASE loss effect in our more detailed modeling of the dye laser system. Careful normalization of our computer codes to the experimental data would also be achieved during Phase II, insuring that all of the important physics effects have been addressed, and that we can rely upon the predictability and accuracy of our codes to further optimize the dye laser design. In order for the device to be useful to the U. S. Army, every effort will be made to arrive at an experimental demonstration that is of a size and configuration of interest. This will be achieved by consultation with the Technical Contract Monitor.

VII. Matching New York State SBIR Program:

In New York State, the New York State Science and Technology Foundation matches the amount of the Federal Phase I award. New York State SBIR programs are also six months in duration. This funding is meant to provide program and personnel continuity between the Federal Phase I and Phase II programs. We intend to take advantage of this funding and improve our analytical tools for the Phase II program.

VIII. References

- [1] G. C. Catella et. al., IEEE JQE 24, 1201 (1988).
- [2] H. Vanherzeele and C. Chen, Appl. Opt. 27, 2634 (1988).
- [3] P. Moulton, private communication.
- [4] Authors unknown, Czech. Jour. Phys., B38 (1988).
- [5] P. Moulton, Tunable Solid State Lasers, Springer-Verlag (1985).
- [6] J. M. Eggleston et. al., IEEE JQE 24, 1009 (1988).
- [7] R. Rapoport, private communication.
- [8] D. Brown, D. Benfey, R. Rapoport, unpublished.
- [9] Methods of Experimental Physics, Vol. 15, Part B, Academic Press (1979).
- [10] M. Rosker and C.L. Tang, JOSA B, 2, 691 (1985).
- [11] M. Rosker et. al., IEEE JQE, QE-21, 1600 (1985).
- [12] H. Vanherzeele et. al., Appl. Optics 27, 3314 (1988).
- [13] Optical Phase Conjugation, R. Fisher ed., Academic Press (1983).
- [14] Dye Lasers, F.P. Schafer ed., Springer Verlag (1978).
- [15] Methods of Experimental Physics, Vol. 15, Part A, Academic Press (1979).
- [16] Principles of Optics, M. Born and E. Wolf, Pergamon Press (1980).
- [17] D.C. Brown et. al., paper presented at Ja Jolla Conference on Tunable Lasers (1984).
- [18] W. Martin and J. Chernoch, US Patent # 3,633,126 (1972).
- [19] L. Schelonka and C. Clayton, Opt. Letters 13, 42 (1988).
- [20] R. Craxton, Opt. Commun. 34, 474 (1980).
- [21] J. Armstrong et. al., Phys. Rev. 127, 1918 (1962).
- [22] C. Lin, IEEE JQE, QE-11, 602 (1975).